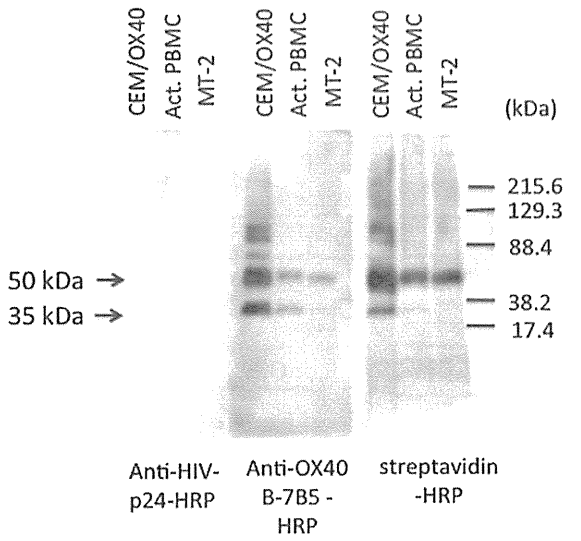

Figure 2 Western blot analysis of OX40. OX40-expressing CEM cells (CEM/OX40), *in vitro* activated PBMCs and MT-2 cells were cell-surface labeled with biotin, lysed and immunoprecipitated with anti-OX40 (B-7B5). The precipitates were subjected to 10% PAGE and blotted onto nitrocellulose sheets. The sheets were then probed with HRP-labeled anti-HIV-1 p24 (as a control), anti-OX40 (B-7B5) or streptavidin. Mol. Wt. markers are shown on the right. Data shown are representative of 3 independent experiments.

addition of soluble rec-OX40L. This inhibition was mediated by OX40L-OX40 interaction since the addition of the anti-OX40L blocking mAb (clone 5A8) and/or the addition of a mixture of the anti-β-chemokine mAbs reversed the level of reduction. It is worthy to note that, similar to data we have previously reported with the use of recombinant OX40L [21], X4 HIV-1 infection was not influenced by co-cultivation with PFA-fixed HTLV-1$^+$ T cell line, suggesting the CCR5-specificity of this antiviral effect.

Finally, we compared the potential of membrane bound OX40L of the fixed HTLV-1$^+$ T cell lines with that of soluble rec-OX40L to inhibit R5 HIV-1 infection by the quantitation of p24 production in the culture supernatants. As shown in Figure 6, whereas the inhibitory effect of the rec-OX40L reached a plateau at levels > 1.25 μg/ml, the autologous HTLV-1$^+$ T cell line could inhibit more effectively at even an HTLV-1$^+$ T cell to PBMCs ratio as low as 0.3. The maximum inhibition reached with rec-OX40 was around 65% of the maximum inhibition reached with HTLV-1$^+$ T cell line, with similar IC_{50}. Altogether, these data demonstrate that indeed, the OX40L expressed by HTLV-1$^+$ T cell lines is biologically active.

Discussion

In the present study, we revealed that the cell surface expressed OX40L on T cell lines immortalized by HTLV-1 is biologically active in concert with the co-expression of an inactive form of OX40. As far as we know, this is the first study to report the polarized "OX40L-active/OX40 inactive" expression by HTLV-1$^+$ T cell lines. The expression of active forms of OX40L is not unique to HTLV-1$^+$ T cell lines, since similar conditions have also been observed in normal T cells when they are activated under mild DNA damaging conditions or cultured for long-term in IL-2 containing media with periodic stimulation [11,24]. However, compared to these normal T cells, HTLV-1$^+$ T cell lines are immortal and thus can provide unlimited amounts of OX40L.

The precise mechanism for the inability of OX40 on HTLV-1$^+$ T cell lines to bind OX40L remains to be clearly defined. Based on our previous paper showing that functional OX40L can be transferred to OX40 intercellularly [25], we hypothesize that the cell surface OX40 may be saturated with endogenously produced OX40L in *cis* and/or *trans* mode. Indeed, the WB analysis showed that the OX40-OX40L blocking mAb W4-54 that did not stain living HTLV-1$^+$ T cells reacted to the p50 OX40 molecule (Additional file 2: Figures S2 and Additional file 3: Figures S3). In accordance with this assumption, we demonstrated the presence of OX40-OX40L complexes in lysates of HTLV-1$^+$ T cell lines by ELISA (Figure 4). It remains unclear why there were significant amounts of OX40L-free OX40 molecules in the lysates from HTLV-1$^+$ T cells as determined by ELISA. It will be highly likely that the detergent treatment dissociates the OX40 and OX40L complex due to perturbation of cytoplasmic membrane structure including lipid rafts on which OX40 is supposed to reside in association with the other TNFR member such as 4-1BB [26,27]. In addition, our preliminary data that supports the OX40 saturation hypothesis includes the finding using the HUT 102 cell line that is another HTLV-1$^+$ T cell line from which the original OX40 gene was cloned [13]. This HUT102 cell line stained with both B-7B5 and W4-54 mAbs, but not with anti-OX40L (5A8 mAb), and was able to bind recombinant OX40L but not OX40 (Additional file 3: Figure S3). Although it is not clear why HUT102 cell line was positive for Tax antigen but negative for OX40L expression, these data clearly showed that in the absence of OX40L, functional OX40 can be expressed on the cell surface. It will be of interest to examine whether the inactive form of the OX40 can be converted to an active form after silencing the expression of OX40L in HTLV-1$^+$ T cell lines. Such studies are currently in progress.

On the basis of the present and previous results on OX40L [21], it can be hypothesized that OX40L may have a therapeutic and prophylactic potential against R5 HIV-1 infection. However, at present, purified biologically active forms of human OX40L protein in large quantities is not available. The alternative is to utilize

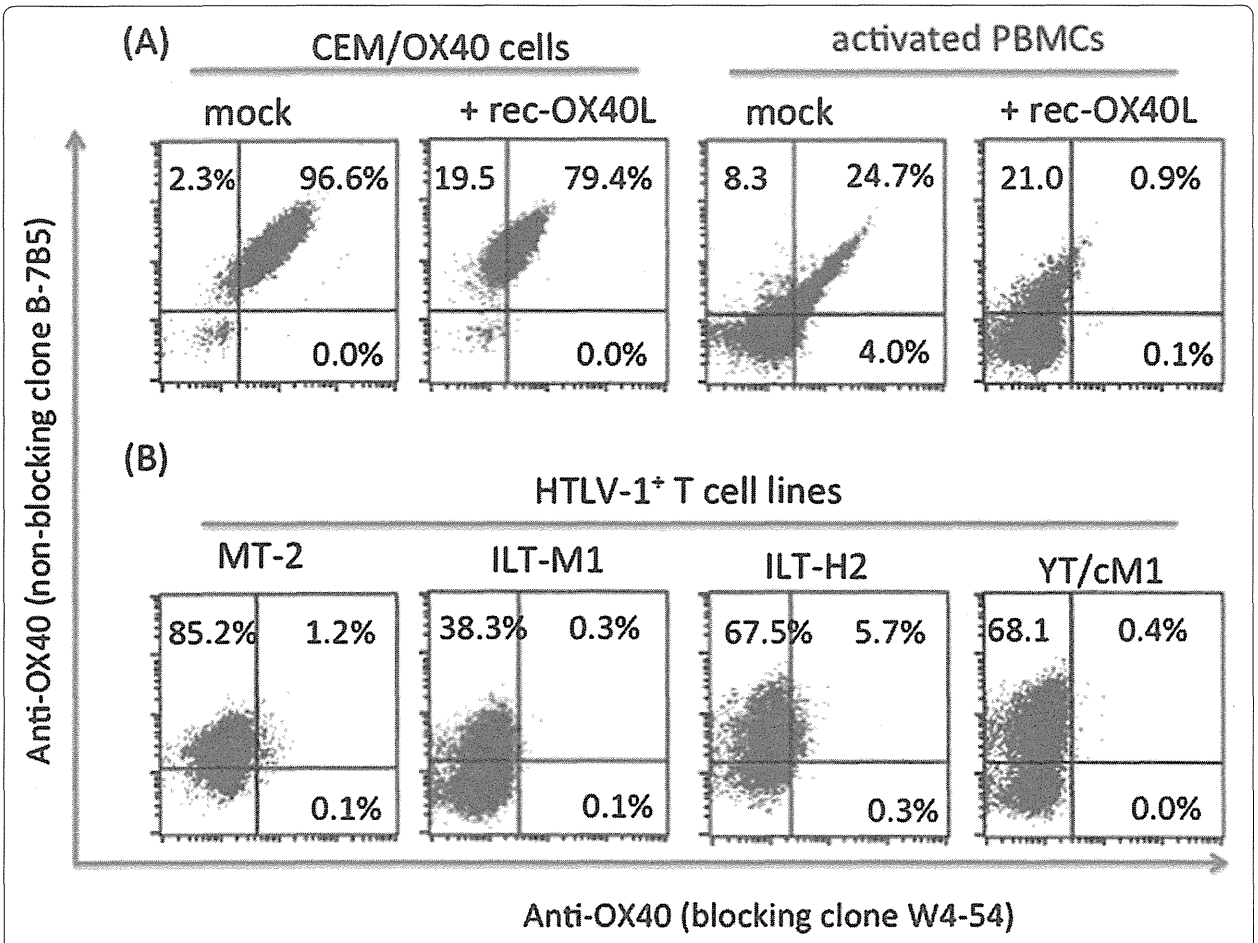

Figure 3 Blocking (clone W4-54) versus non-blocking (clone B-7B5) mAb against 2 distinct epitopes of OX40 distinguish between OX40L bound and unbound OX40. (A) OX40-expressing CEM and activated PBMCs were stained with the two mAbs in the absence (mock) or presence of 1 μg/ml of recombinant OX40L (rec-OX40L). **(B)** Various HTLV-1$^+$ T cell lines were stained with B-7B5 andW4-54 labeled with FITC and Cy5, respectively. Data shown are representative of 3 independent experiments.

OX40L-fusion proteins [28], OX40L-expressing recombinant virus [20], OX40L mRNA-transfected cells [29], lentivirus-transduced DCs [30], or autologous dying normal T cells [24]. The superiority of using cell membrane-bound OX40L as compared with the use of a soluble form was documented by data observed by the degree of inhibition of R5 HIV-1 as seen in the present study (Figure 6). These findings are in accord with a previous study that showed that the membrane-immobilized form of OX40L is highly active in the stimulation of an OX40-transfected cell line to produce cytokines [31]. In addition to OX40L, HTLV-1$^+$ cell lines may exert additional suppressing effect on R5 HIV-1 infection via Tax protein, since Tax proteins of HTLV-1 and HTLV-2 have been shown to play a role in generating antiviral responses against HIV-1 via induction of CCR5-binding chemokines *in vitro* [32]. This view is supported by the finding that co-infection with HTLV interferes with the progression of HIV-1 disease *in vivo* [33]. However, such Tax effects in the present study may be less potent than OX40L since anti-OX40L mAb significantly reversed the suppression of R5-HIV-1 induced by co-culture with autologous HTLV-1$^+$ T cell lines (Figure 5).

Conclusions

The present results demonstrate that HTLV-1$^+$ T cell line is a unique source of functional human OX40L, and suggest that autologous HTLV-1-immortalized T cell lines can be utilized as a conventional source of natural and functional OX40L in large quantities for various immunological studies.

Methods

Reagents

The medium used throughout the studies consisted of RPMI 1640 medium (Sigma-Aldrich. Inc. St. Louis, MO), supplemented with 10% fetal calf serum (FCS), 100 U/ml

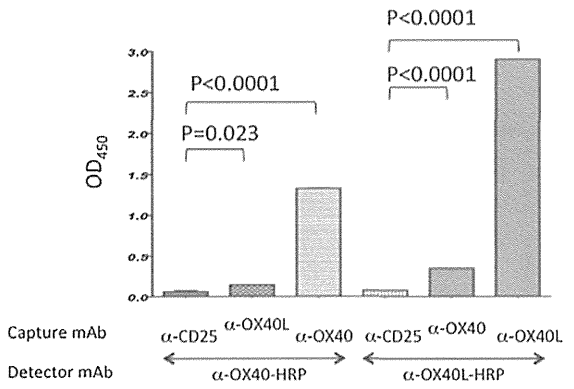

Figure 4 Presence of OX40-OX40L complexes in HTLV-1$^+$ T cell lysates. The ILT-H2 cell line derived from an ATL patient were lysed and the lysates incubated in microtiter wells that had been previously coated with either anti-CD25, OX40 or OX40L mAb for 1 hour. Anti-CD25 mAb was used as a non-specific negative control. After washing, the levels of OX40 or OX40L bound to the plates were assayed using either HRP-labeled anti-OX40 or anti-OX40L mAb. Data shown are representative of 3 independent experiments.

penicillin and 100 μg/ml streptomycin (hereinafter called RPMI medium). Anti-human CD3 mAb (clone OKT-3) and agonistic anti-CD28 mAb were purchased from the American Type Culture Collection (Rockville, MD) and Biolegend (San Diego, CA), respectively. Neutralizing mAbs against human RANTES, MIP-1α, and MIP-1β were purchased from R&D systems (Minneapolis, MN). The mouse mAbs produced in our laboratory included anti-OX40L (blocking clone 5A8 [34] and clone HD1, unpublished), anti-human OX40 (non-blocking clone B-7B5 and clone 17D8 [35]), anti-HIV-1 p24 (clones NP-24 and 2C2 [21]) and anti-CD25 (clone H-8) [36]. The rat mAbs included anti-human OX40 (blocking clone W4-54) and anti-HCV (clone Mo-8) [25,37]). Some clones were labeled with HRP using a kit (Dojin, Kumamoto, Japan) and used as the detector mAb in ELISA. These in-house mAbs were isolated from ascites fluid prepared in Balb/c or CB.17-SCID mice. The IgGs were purified utilizing a standard gel filtration method. Some of them were labeled with FITC, HiLyte Fluor 647 or Cy5 using commercial labeling kits (Dojin, GE Healthcare) according to the manufacturer's instructions. Biotinylated recombinant-soluble human OX40 (sOX40 in a form of murine IgG2a-Fc fusion protein) and OX40L (sOX40L in a form of murine CD8-fusion protein) were purchased from Ancell (Bayport, MN) and used with PE-streptavidin (BioLegend) for staining. Unlabeled glycosylated recombinant human OX40L that consists of OX40L with a human CD33 signal peptide produced in NS1 cells was purchased from R&D systems. Human recombinant IL-2 was obtained as a courtesy from the NIH-AIDS Reagent and Repository program (Bethesda, MD).

Cell lines

The HTLV-1-producing T cell lines used included the MT-2, HUT102 and the IL-2 dependent T cell lines ILT-M1 and ILT-H2 that had been generated from a HTLV-1-associated myelopathy (HAM) and an adult T cell leukemia (ATL) patient, respectively. Additional cell lines utilized included the CEM cell lines transfected with either human OX40L or OX40 (CEM/OX40L and CEM/OX40) [38]. T cells isolated from normal human donors were immortalized by HTLV-1 as follows.

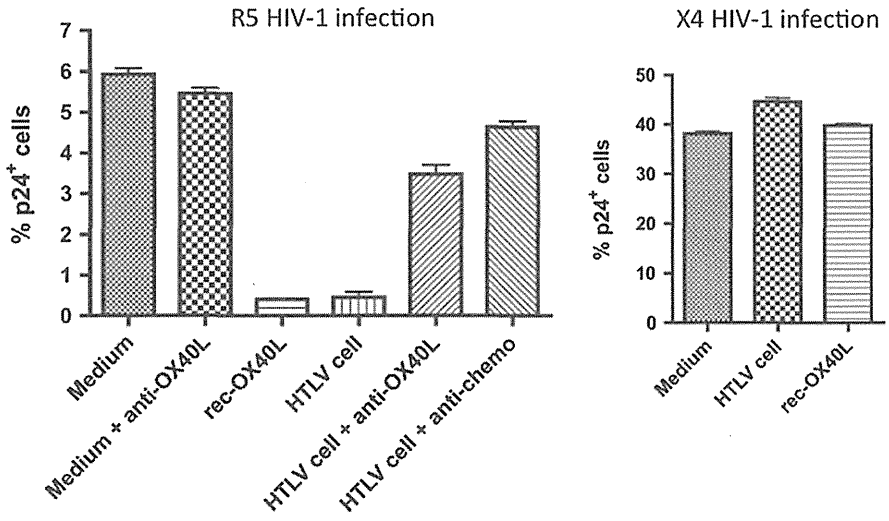

Figure 5 PFA-inactivated HTLV-1$^+$ T cells inhibit infection of activated autologous PBMCs with R5 HIV-1, but not X4 HIV-1, via OX40L and β-chemokines. In vitro activated PBMCs were infected with either R5 HIV-1 (JR-FL strain) or X4 HIV-1 (NL4-3 strain) and cultured in the presence or absence of recombinant OX40L, PFA-inactivated autologous HTLV-1$^+$ T cells, anti-OX40L blocking mAb (5A8) or a mixture of anti-β-chemokine neutralizing mAbs. After 4 days, the cells were examined for intracellular HIV-1 p24 by FCM. Data shown are representative of 3 independent experiments.

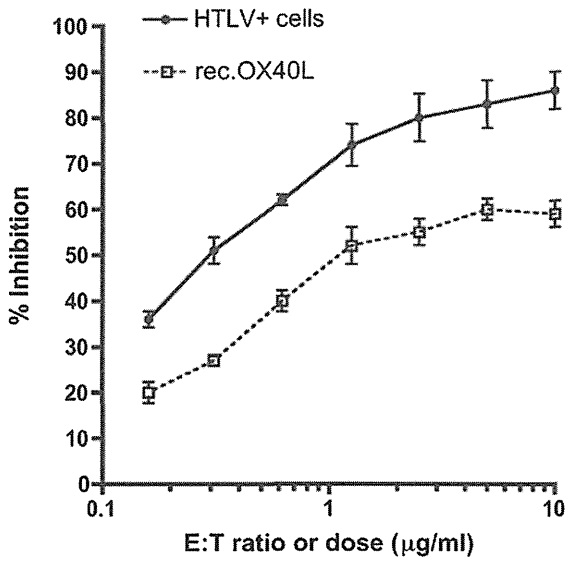

Figure 6 HTLV-1$^+$ T cells are more potent in the inhibition of R5 HIV-1 infection than recombinant soluble OX40L. R5 HIV-1-infected PBMCs prepared as in Figure 5 were cultured in the presence or absence of a graded concentration of recombinant soluble OX40L or PFA-fixed autologous HTLV-1$^+$ T cells. After 4 days, the levels of p24 produced in the culture supernatants were quantitated by ELISA. Data shown are representative of 2 independent experiments.

PBMCs from healthy donors were obtained by density gradient centrifugation of heparinized whole blood on HistoPAQUE-1077 (Sigma-Aldrich), suspended at 2 × 10^6 cells/ml in RPMI medium, dispensed into individual wells of 24-well plates (BD) (1 ml/well) pre-coated with 5 μg/ml OKT3 for 1 hour and cultured in the presence of soluble 0.1 μg/ml anti-CD28 mAb. After 24 hours at 37°C in a 5% CO_2 humidified atmosphere, the activated PBMCs were harvested and washed once. These activated PBMCs (1 × 10^6 cells/ml) were mixed with an equal number of ILT-M1 cells that were pretreated with 50 μg/ml MMC for 30 min at 37°C and cultured in RPMI media supplemented with 20 U/ml IL-2 (culture media). The cultures were performed in 24-well plates (BD) (2 ml/well) and the culture media was replenished every 3–4 days. After 1 ~ 2 months when HTLV-1 Tax$^+$ T cells appeared and started to grow continuously, they were split every 3 to 5 days using the culture medium.

Flow Cytometry (FCM)

FCM analysis of live cells was carried out as described previously. Briefly, cells to be analyzed were Fc-blocked with 2 mg/ml normal human pooled IgG on ice for 15 min. Aliquots of these cells were then subjected to staining using pre-determined optimum concentrations of fluorescent dye-conjugated mAbs for 30 min on ice. The cells were then washed using FACS buffer (PBS containing 2% FCS and 0.1% sodium azide), fixed in 1% paraformaldehyde (PFA) containing FACS buffer and analyzed using a FACS Calibur, and the data obtained were analyzed using the Cell Quest software (BD). In order to determine whether cell surface OX40 or OX40L is functional, aliquots of Fc-blocked cells were incubated with either biotinylated recombinant-OX40L (rec-OX40L) or rec-OX40 at a concentration of 2.5 μg/ml for 30 minutes on ice, followed by staining with PE-labeled streptavidin (Beckman Coulter) for 30 minutes on ice and then analyzed by FCM. For detection of HIV-1 infected cells, PBMCs were fixed with PBS containing 4% PFA followed by washing twice in FACS buffer containing 0.5% saponin. These cells were Fc-blocked with 2 mg/ml normal human pooled IgG on ice for 15 min, and aliquots of these cells were stained with FITC- or Cy5-conjugated anti-HIV-1 p24 mAb (clone 2C2) for 30 min on ice. The cells were then washed using FACS buffer and absolute cell counts of p24$^+$ cells were performed by FCM using a cell counting kit (BD) according to the manufacturer's protocol. For staining of Tax antigen, cells were fixed with PBS containing 4% PFA followed by washing in FACS buffer containing 0.5% saponin. Aliquots of these cells were stained with Cy5-conjugated mouse anti-Tax mAb (Lt-4) [39] for 30 min on ice.

ELISA and Western blot

For the quantitation of OX40L and OX40 by ELISA, anti-OX40L capture mAb (clone HD1)/ HRP-labeled detector mAb (clone 8F4) and anti-OX40 (clone B-7B5)/ HRP-labeled detector mAb (clone 17D8), respectively, were used together with recombinant standard proteins purchased from R&D systems. Immunoprecipitation followed by Western blot analysis of OX40 was performed as reported previously [40].

HIV-1 preparation and infection

HIV-$1_{JR\text{-}FL}$ and HIV-$1_{NL4\text{-}3}$ viral stocks were produced as described previously [21]. *In vitro* activated PBMCs were prepared as described above, washed once and infected with either R5 HIV-$1_{JR\text{-}FL}$ or X4 HIV-$1_{NL4\text{-}3}$ at a multiplicity of infection (m.o.i.) of 0.005 for 2 hours. After washing 3 times, PBMCs were re-suspended at 1 × 10^6 cells/ml in 20 U/ml IL-2-containing RPMI medium, dispensed into individual wells of 48-well plates (BD) (0.5 ml/well) and cultured in the presence or absence of 1 μg/ml of rec-OX40L or graded numbers of autologous HTLV-1$^+$ T cells (HTLV-1$^+$ T cells : PBMCs ratio of 10 to 0.15) that had been previously inactivated with 4% paraformaldehyde (PFA). Production of HIV-1 was determined by either the measurement of HIV-1 core p24 levels produced in the culture supernatants using our in-house formulated and standardized kits or FCM using Cy5 labeled anti-HIV-1 p24 mAb [21].

Statistical analysis

Data were tested for significance using the Student's *t* test by using Prism software (GraphPad Software).

Additional files

Additional file 1: Figure S1. Characterization of two anti-human OX40 mAbs. In the presence of B-7B5, W4-54 or isotype control mAbs, the OX40 and OX40L co-expressing control CEM cells were singly stained either with biotinylated recombinant OX40L (rec-OX40L) or rec-OX40, respectively, followed by PE-streptavidin. Data shown are representative profiles of 3 independent experiments.

Additional file 2: Figure S2. Detection of OX40 expressed by HTLV-1$^+$ T cell line (YT/cM1) by Western Blot with B-7B5 and W4-54 mAbs. Cell lysates of HTLV-1$^+$ T cell line, YT/cM1, were subjected to 10% PAGE and blotted onto nitrocellulose sheets. The sheets were then probed with anti-OX40 mAbs (B-7B5 or W4-54) or isotype controls followed by goat anti-mouse IgG or anti-rat IgG. Mol. Wt. markers are shown on the right. Data shown are representative of 2 independent experiments.

Additional file 3: Figure S3. Phenotype of HUT-102 cell line. Phenotype of HUT-102 cells were examined by FCM using anti-OX40 mAbs (FITC-labeled B-7B5 and Cy5-labeled W4-54), anti-OX40L (Cy5-labeled 5A8), biotinylated OX40 (rec-OX40) and OX40L (rec-OX40L) followed by PE-streptavidin. Intracellular Tax antigen was stained by mouse anti-Tax Lt-4 mAb.

Competing interests

The authors declare no competing financial interests.

Authors' contributions

DK and YTak generated HTLV-1$^+$ T cell lines and carried out the FCM and ELISA, performed the statistical analysis and drafted the manuscript. AT performed WB and FCM analyses. AK produced R5 and X4 HIV-1 and titrated. RT produced and labeled antibodies, confirmed their specificities and made in-house ELISA. AAA participated in the design of the study and helped to draft the manuscript. YT conceived of the study, participated in its design and coordination, carried out the HIV-1 infection experiments and drafted the manuscript. All authors read and approved the final manuscript.

Acknowledgements

This work was supported by grants from a Grant-in-Aid from the Ministry of Health, Labor and Welfare of Japan.

Author details

[1]Department of Immunology, Graduate School of Medicine, University of the Ryukyus, Okinawa 903-0215, Japan. [2]Department of Pathology, Emory University School of Medicine, Atlanta, GA 30322, USA.

Received: 10 June 2013 Accepted: 12 November 2013
Published: 18 November 2013

References

1. Ishii N, Takahashi T, Soroosh P, Sugamura K: **OX40-OX40 ligand interaction in T-cell-mediated immunity and immunopathology.** *Adv Immunol* 2010, 105:63–98.
2. Croft M, Duan W, Choi H, Eun SY, Madireddi S, Mehta A: **TNF superfamily in inflammatory disease: translating basic insights.** *Trends Immunol* 2012, 33:144–152.
3. Tanaka Y, Inoi T, Tozawa H, Yamamoto N, Hinuma Y: **A glycoprotein antigen detected with new monoclonal antibodies on the surface of human lymphocytes infected with human T-cell leukemia virus type-I (HTLV-I).** *Int J Cancer* 1985, 36:549–555.
4. Miura S, Ohtani K, Numata N, Niki M, Ohbo K, Ina Y, Gojobori T, Tanaka Y, Tozawa H, Nakamura M, *et al*: **Molecular cloning and characterization of a novel glycoprotein, gp34, that is specifically induced by the human T-cell leukemia virus type I transactivator p40tax.** *Mol Cell Biol* 1991, 11:1313–1325.
5. Ohshima Y, Tanaka Y, Tozawa H, Takahashi Y, Maliszewski C, Delespesse G: **Expression and function of OX40 ligand on human dendritic cells.** *J Immunol* 1997, 159:3838–3848.
6. Baum PR, Gayle RB 3rd, Ramsdell F, Srinivasan S, Sorensen RA, Watson ML, Seldin MF, Clifford KN, Grabstein K, Alderson MR, *et al*: **Identification of OX40 ligand and preliminary characterization of its activities on OX40 receptor.** *Circ Shock* 1994, 44:30–34.
7. Zingoni A, Sornasse T, Cocks BG, Tanaka Y, Santoni A, Lanier LL: **Cross-talk between activated human NK cells and CD4+ T cells via OX40-OX40 ligand interactions.** *J Immunol* 2004, 173:3716–3724.
8. Kotani A, Hori T, Fujita T, Kambe N, Matsumura Y, Ishikawa T, Miyachi Y, Nagai K, Tanaka Y, Uchiyama T: **Involvement of OX40 ligand + mast cells in chronic GVHD after allogeneic hematopoietic stem cell transplantation.** *Bone Marrow Transplant* 2007, 39:373–375.
9. Imura A, Hori T, Imada K, Kawamata S, Tanaka Y, Imamura S, Uchiyama T: **OX40 expressed on fresh leukemic cells from adult T-cell leukemia patients mediates cell adhesion to vascular endothelial cells: implication for the possible involvement of OX40 in leukemic cell infiltration.** *Blood* 1997, 89:2951–2958.
10. Takasawa N, Ishii N, Higashimura N, Murata K, Tanaka Y, Nakamura M, Sasaki T, Sugamura K: **Expression of gp34 (OX40 ligand) and OX40 on human T cell clones.** *Jpn J Cancer Res* 2001, 92:377–382.
11. Kondo K, Okuma K, Tanaka R, Zhang LF, Kodama A, Takahashi Y, Yamamoto N, Ansari AA, Tanaka Y: **Requirements for the functional expression of OX40 ligand on human activated CD4+ and CD8+ T cells.** *Hum Immunol* 2007, 68:563–571.
12. Croft M: **Control of immunity by the TNFR-related molecule OX40 (CD134).** *Annu Rev Immunol* 2010, 28:57–78.
13. Latza U, Durkop H, Schnittger S, Ringeling J, Eitelbach F, Hummel M, Fonatsch C, Stein H: **The human OX40 homolog: cDNA structure, expression and chromosomal assignment of the ACT35 antigen.** *Eur J Immunol* 1994, 24:677–683.
14. Baum PR, Gayle RB 3rd, Ramsdell F, Srinivasan S, Sorensen RA, Watson ML, Seldin MF, Baker E, Sutherland GR, Clifford KN, *et al*: **Molecular characterization of murine and human OX40/OX40 ligand systems: identification of a human OX40 ligand as the HTLV-1-regulated protein gp34.** *EMBO J* 1994, 13:3992–4001.
15. Weinberg AD, Evans DE, Thalhofer C, Shi T, Prell RA: **The generation of T cell memory: a review describing the molecular and cellular events following OX40 (CD134) engagement.** *J Leukoc Biol* 2004, 75:962–972.
16. Compaan DM, Hymowitz SG: **The crystal structure of the costimulatory OX40-OX40L complex.** *Structure* 2006, 14:1321–1330.
17. Imura A, Hori T, Imada K, Ishikawa T, Tanaka Y, Maeda M, Imamura S, Uchiyama T: **The human OX40/gp34 system directly mediates adhesion of activated T cells to vascular endothelial cells.** *J Exp Med* 1996, 183:2185–2195.
18. Weinberg AD: **OX40: targeted immunotherapy–implications for tempering autoimmunity and enhancing vaccines.** *Trends Immunol* 2002, 23:102–109.
19. Croft M, So T, Duan W, Soroosh P: **The significance of OX40 and OX40L to T-cell biology and immune disease.** *Immunol Rev* 2009, 229:173–191.
20. Liu J, Ngai N, Stone GW, Yue FY, Ostrowski MA: **The adjuvancy of OX40 ligand (CD252) on an HIV-1 canarypox vaccine.** *Vaccine* 2009, 27:5077–5084.
21. Tanaka R, Takahashi Y, Kodama A, Saito M, Ansari AA, Tanaka Y: **Suppression of CCR5-tropic HIV type 1 infection by OX40 stimulation via enhanced production of beta-chemokines.** *AIDS Res Hum Retroviruses* 2010, 26:1147–1154.
22. Higashimura N, Takasawa N, Tanaka Y, Nakamura M, Sugamura K: **Induction of OX40, a receptor of gp34, on T cells by trans-acting transcriptional activator, Tax, of human T-cell leukemia virus type I.** *Jpn J Cancer Res* 1996, 87:227–231.
23. Pichler K, Kattan T, Gentzsch J, Kress AK, Taylor GP, Bangham CR, Grassmann R: **Strong induction of 4-1BB, a growth and survival promoting costimulatory receptor, in HTLV-1-infected cultured and patients' T cells by the viral tax oncoprotein.** *Blood* 2008, 111:4741–4751.
24. Kondo K, Okuma K, Tanaka R, Matsuzaki G, Ansari AA, Tanaka Y: **Rapid induction of OX40 ligand on primary T cells activated under DNA-damaging conditions.** *Hum Immunol* 2008, 69:533–542.
25. Baba E, Takahashi Y, Lichtenfeld J, Tanaka R, Yoshida A, Sugamura K, Yamamoto N, Tanaka Y: **Functional CD4 T cells after intercellular molecular transfer of 0X40 ligand.** *J Immunol* 2001, 167:875–883.

26. Nam KO, Kang H, Shin SM, Cho KH, Kwon B, Kwon BS, Kim SJ, Lee HW: **Cross-linking of 4-1BB activates TCR-signaling pathways in CD8+ T lymphocytes.** *J Immunol* 2005, **174**:1898–1905.
27. Ma BY, Mikolajczak SA, Danesh A, Hosiawa KA, Cameron CM, Takaori-Kondo A, Uchiyama T, Kelvin DJ, Ochi A: **The expression and the regulatory role of OX40 and 4-1BB heterodimer in activated human T cells.** *Blood* 2005, **106**:2002–2010.
28. Taylor L, Bachler M, Duncan I, Keen S, Fallon R, Mair C, McDonald TT, Schwarz H: **In vitro and in vivo activities of OX40 (CD134)-IgG fusion protein isoforms with different levels of immune-effector functions.** *J Leukoc Biol* 2002, **72**:522–529.
29. Dannull J, Nair S, Su Z, Boczkowski D, DeBeck C, Yang B, Gilboa E, Vieweg J: **Enhancing the immunostimulatory function of dendritic cells by transfection with mRNA encoding OX40 ligand.** *Blood* 2005, **105**:3206–3213.
30. Tateyama M, Fujihara K, Ishii N, Sugamura K, Onodera Y, Itoyama Y: **Expression of OX40 in muscles of polymyositis and granulomatous myopathy.** *J Neurol Sci* 2002, **194**:29–34.
31. Muller N, Wyzgol A, Munkel S, Pfizenmaier K, Wajant H: **Activity of soluble OX40 ligand is enhanced by oligomerization and cell surface immobilization.** *FEBS J* 2008, **275**:2296–2304.
32. Barrios CS, Castillo L, Giam CZ, Wu L, Beilke MA: **Inhibition of HIV Type 1 replication by human T lymphotropic virus Types 1 and 2 Tax Proteins in Vitro.** *AIDS Res Hum Retroviruses* 2013, **29**:1061–1067.
33. Beilke MA: **Retroviral coinfections: HIV and HTLV: taking stock of more than a quarter century of research.** *AIDS Res Hum Retroviruses* 2012, **28**:139–147.
34. Tozawa H, Andoh S, Takayama Y, Tanaka Y, Lee B, Nakamura H, Hayami M, Hinuma Y: **Species-dependent antigenicity of the 34-kDa glycoprotein found on the membrane of various primate lymphocytes transformed by human T-cell leukemia virus type-I (HTLV-I) and simian T-cell leukemia virus (STLV-I).** *Int J Cancer* 1988, **41**:231–238.
35. Takahashi Y, Tanaka R, Yamamoto N, Tanaka Y: **Enhancement of OX40-induced apoptosis by TNF coactivation in OX40-expressing T cell lines in vitro leading to decreased targets for HIV type 1 production.** *AIDS Res Hum Retroviruses* 2008, **24**:423–435.
36. Tanaka Y, Inoi T, Tozawa H, Sugamura K, Hinuma Y: **New monoclonal antibodies that define multiple epitopes and a human-specific marker on the interleukin 2 receptor molecules of primates.** *Microbiol Immunol* 1986, **30**:373–388.
37. Inudoh M, Kato N, Tanaka Y: **New monoclonal antibodies against a recombinant second envelope protein of Hepatitis C virus.** *Microbiol Immunol* 1998, **42**:875–877.
38. Takahashi Y, Tanaka Y, Yamashita A, Koyanagi Y, Nakamura M, Yamamoto N: **OX40 stimulation by gp34/OX40 ligand enhances productive human immunodeficiency virus type 1 infection.** *J Virol* 2001, **75**:6748–6757.
39. Lee B, Tanaka Y, Tozawa H: **Monoclonal antibody defining tax protein of human T-cell leukemia virus type-I.** *Tohoku J Exp Med* 1989, **157**:1–11.
40. Tanaka R, Yoshida A, Murakami T, Baba E, Lichtenfeld J, Omori T, Kimura T, Tsurutani N, Fujii N, Wang ZX, *et al*: **Unique monoclonal antibody recognizing the third extracellular loop of CXCR4 induces lymphocyte agglutination and enhances human immunodeficiency virus type 1-mediated syncytium formation and productive infection.** *J Virol* 2001, **75**:11534–11543.

doi:10.1186/1743-422X-10-338
Cite this article as: Kasahara *et al.*: Natural OX40L expressed on human T cell leukemia virus type-I-immortalized T cell lines interferes with infection of activated peripheral blood mononuclear cells by CCR5-utilizing human immunodeficiency virus. *Virology Journal* 2013 **10**:338.

HIV-1 Vpr Accelerates Viral Replication during Acute Infection by Exploitation of Proliferating CD4$^+$ T Cells *In Vivo*

Kei Sato[1,2]*, Naoko Misawa[1], Shingo Iwami[3,4], Yorifumi Satou[5], Masao Matsuoka[5], Yukihito Ishizaka[6], Mamoru Ito[7], Kazuyuki Aihara[8,9], Dong Sung An[10,11,12], Yoshio Koyanagi[1,2]*

1 Laboratory of Virus Pathogenesis, Institute for Virus Research, Kyoto University, Kyoto, Kyoto, Japan, **2** Center for Emerging Virus Research, Institute for Virus Research, Kyoto University, Kyoto, Kyoto, Japan, **3** Department of Biology, Faculty of Sciences, Kyushu University, Fukuoka, Fukuoka, Japan, **4** Precursory Research for Embryonic Science and Technology (PRESTO), Japan Science and Technology Agency (JST), Kawaguchi, Saitama, Japan, **5** Laboratory of Viral Control, Institute for Virus Research, Kyoto University, Kyoto, Kyoto, Japan, **6** Department of Intractable Diseases, National Center for Global Health and Medicine, Shinjuku-ku, Tokyo, Japan, **7** Central Institute for Experimental Animals, Kawasaki, Kanagawa, Japan, **8** Institute of Industrial Science, The University of Tokyo, Meguro-ku, Tokyo, Japan, **9** Graduate School of Information Science and Technology, The University of Tokyo, Meguro-ku, Tokyo, Japan, **10** Division of Hematology-Oncology, University of California, Los Angeles (UCLA), Los Angeles, California, United States of America, **11** School of Nursing, UCLA, Los Angeles, California, United States of America, **12** AIDS Institute, UCLA, Los Angeles, California, United States of America

Abstract

The precise role of viral protein R (Vpr), an HIV-1-encoded protein, during HIV-1 infection and its contribution to the development of AIDS remain unclear. Previous reports have shown that Vpr has the ability to cause G_2 cell cycle arrest and apoptosis in HIV-1-infected cells *in vitro*. In addition, *vpr* is highly conserved in transmitted/founder HIV-1s and in all primate lentiviruses, which are evolutionarily related to HIV-1. Although these findings suggest an important role of Vpr in HIV-1 pathogenesis, its direct evidence *in vivo* has not been shown. Here, by using a human hematopoietic stem cell-transplanted humanized mouse model, we demonstrated that Vpr causes G_2 cell cycle arrest and apoptosis predominantly in proliferating CCR5$^+$ CD4$^+$ T cells, which mainly consist of regulatory CD4$^+$ T cells (Tregs), resulting in Treg depletion and enhanced virus production during acute infection. The Vpr-dependent enhancement of virus replication and Treg depletion is observed in CCR5-tropic but not CXCR4-tropic HIV-1-infected mice, suggesting that these effects are dependent on the coreceptor usage by HIV-1. Immune activation was observed in CCR5-tropic wild-type but not in *vpr*-deficient HIV-1-infected humanized mice. When humanized mice were treated with denileukin diftitox (DD), to deplete Tregs, DD-treated humanized mice showed massive activation/proliferation of memory T cells compared to the untreated group. This activation/proliferation enhanced CCR5 expression in memory CD4$^+$ T cells and rendered them more susceptible to CCR5-tropic wild-type HIV-1 infection than to *vpr*-deficient virus. Taken together, these results suggest that Vpr takes advantage of proliferating CCR5$^+$ CD4$^+$ T cells for enhancing viremia of CCR5-tropic HIV-1. Because Tregs exist in a higher cycling state than other T cell subsets, Tregs appear to be more vulnerable to exploitation by Vpr during acute HIV-1 infection.

Citation: Sato K, Misawa N, Iwami S, Satou Y, Matsuoka M, et al. (2013) HIV-1 Vpr Accelerates Viral Replication during Acute Infection by Exploitation of Proliferating CD4$^+$ T Cells *In Vivo*. PLoS Pathog 9(12): e1003812. doi:10.1371/journal.ppat.1003812

Editor: Jeremy Luban, University of Massachusetts Medical School, United States of America

Received June 17, 2013; **Accepted** October 22, 2013; **Published** December 5, 2013

Funding: This work was supported in part by grants from the following: Grants-in-Aid for Scientific Research B21390137 (to YK) and S22220007 (to MI and YK) and a Grant-in-Aid for Young Scientists B23790500 (to KS) from the Japan Society for the Promotion of Science (JSPS); grants from Research on Emerging and Reemerging Infectious Diseases (to YK) and Research on HIV/AIDS (to YK) from the Ministry of Health, Labor and Welfare of Japan; a grant from the Uehara Memorial Foundation (to KS); the Shimizu Foundation for Immunological Research Grant (to KS); Takeda Science Foundation (to KS); JST PRESTO program (to SI); and a UCLA CFAR grant 5P30AI028697 (to DSA). This research was also supported by the Aihara Innovative Mathematical Modelling Project, JSPS through the "Funding Program for World-Leading Innovative R&D on Science and Technology (FIRST Program)," initiated by the Council for Science and Technology Policy (to KS, SI, and KA). The funders had no role in study design, data collection and analysis, decision to publish, or preparation of the manuscript.

Competing Interests: The authors have declared that no competing interests exist.

* E-mail: ksato@virus.kyoto-u.ac.jp (KS); ykoyanag@virus.kyoto-u.ac.jp (YK)

Introduction

Human immunodeficiency virus type 1 (HIV-1), the causative agent of acquired immunodeficiency syndrome (AIDS), encodes four viral accessory proteins: Vif, Vpu, Nef, and Vpr. Vpr is a small (96 amino acids) but multipotent protein which is known to induce G_2 cell cycle arrest, apoptosis, and the enhancement of HIV-1 long terminal repeat (LTR)-driven transcription in infected cells [1]. Previous *in vitro* studies have reported that *vpr*-deficient HIV-1 is less replicative in CD4$^+$ T cell lines [2] and cycling primary CD4$^+$ T cells [3]. On the other hand, *vpr* deficiency modestly affects viral replication kinetics in tonsil histocultures in which resting CD4$^+$ T cells dominantly reside [4]. *In vivo*, *vpr*-deficient SIV is less replicative but induces AIDS in macaque monkeys [5]. However, although the underlying molecular mechanisms of Vpr function have been widely investigated, the significance and the precise role(s) of Vpr *in vivo* remain unclear.

The main target of HIV-1 *in vivo* is CD4$^+$ T cells. Based on their function and phenotype, primary CD4$^+$ T cells are classified into three subsets: naive CD4$^+$ T cells (Tns), memory CD4$^+$ T cells (Tms), and regulatory CD4$^+$ T cells (Tregs). It is speculated that such phenotypic and functional differences among these subsets

Author Summary

HIV-1 encodes nine genes, five of which (*gag*, *pol*, *env*, *tat*, and *rev*) are essential for viral replication, and four, termed accessory genes (*vif*, *vpu*, *nef*, and *vpr*), appear to aid virus infection. Of the four accessory proteins, Vpr is the most enigmatic. It is well known that Vpr has the potential to cause G_2 cell cycle arrest and apoptosis *in vitro*. Moreover, it has been reported that Vpr-mediated G_2 arrest increases HIV-1 production *in vitro*. However, the role of Vpr in HIV-1 propagation *in vivo* remains unclear. Here, by using a humanized mouse model, we demonstrate that Vpr enhances CCR5-tropic but not CXCR4-tropic HIV-1 replication *in vivo* by exploiting Tregs during acute infection. In CCR5-tropic HIV-1-infected humanized mice, Vpr-dependent G_2 cell cycle arrest and apoptosis are predominantly observed in infected Tregs, and wild-type but not *vpr*-deficient HIV-1-infected mice displayed acute Treg depletion. This Vpr-dependent Treg depletion may lead to immune activation and provide a pool of activated/proliferating $CD4^+$ T cells, which supports subsequent HIV-1 expansion *in vivo*. This is the first report demonstrating the role of Vpr in HIV-1 infection *in vivo*.

closely associates with the infectivitiy, productivity, and replicativity of HIV-1 [6]. However, since cultured primary $CD4^+$ T cell subsets do not retain all of their *in vivo* attributes, the dynamics of each subset on HIV-1 infection are poorly understood.

Among the $CD4^+$ T cell subsets, Tregs constitute 5–10% of all $CD4^+$ T cells in human, monkey, and mouse species [7]. The potential and phenotype of Tregs are under the control of a transcription factor called forkhead box P3 (FOXP3), which is exclusively expressed in Tregs [8]. Tregs are more actively proliferating *in vivo* than the other $CD4^+$ T cell subsets [9–11]. It is well known that Tregs play a central role in the maintenance of self-tolerance and immune homeostasis [7]. In addition, it is implicated that Tregs are closely associated with immunopathological events such as autoimmune diseases [7] and infectious diseases [12–14]. In particular, there are lines of reports showing that HIV-1/SIV infection decreases Tregs in HIV-1-infected patients [15–17] and simian immunodeficiency virus (SIV)-infected macaque monkeys [18–20].

In this study, we infect a human hematopoietic stem cell (HSC)-transplanted humanized mouse model [21–25] with wild-type (WT) and *vpr*-deficient HIV-1 and investigate the fundamental role of Vpr in HIV-1 infection *in vivo*. Our findings suggest that Vpr plays a crucial role in accelerating CCR5-tropic (R5) but not CXCR4-tropic (X4) HIV-1 propagation during acute infection by utilizing $CCR5^+$ proliferating $CD4^+$ T cells including Tregs.

Results

Tregs are depleted during the acute phase of R5 HIV-1 infection

We first characterized the profile of human $CD4^+$ T cell subsets, including Tns, Tms, and Tregs, in human peripheral blood mononuclear cells (PBMCs) isolated from HIV-1-negative healthy donors and in the spleen of humanized mice [21–23]. As shown in Figure 1A, we detected 6.3±0.2% $FOXP3^+$ $CD4^+$ T cells in splenic human $CD4^+$ T cells of humanized mice, which was comparable to those in human peripheral $CD4^+$ T cells (5.4±0.6%; Figure 1B). Consistent with previous reports [26–29], we also confirmed that the phenotypes of Tregs including the expression levels of CD25, CD127, and cytotoxic T-lymphocyte

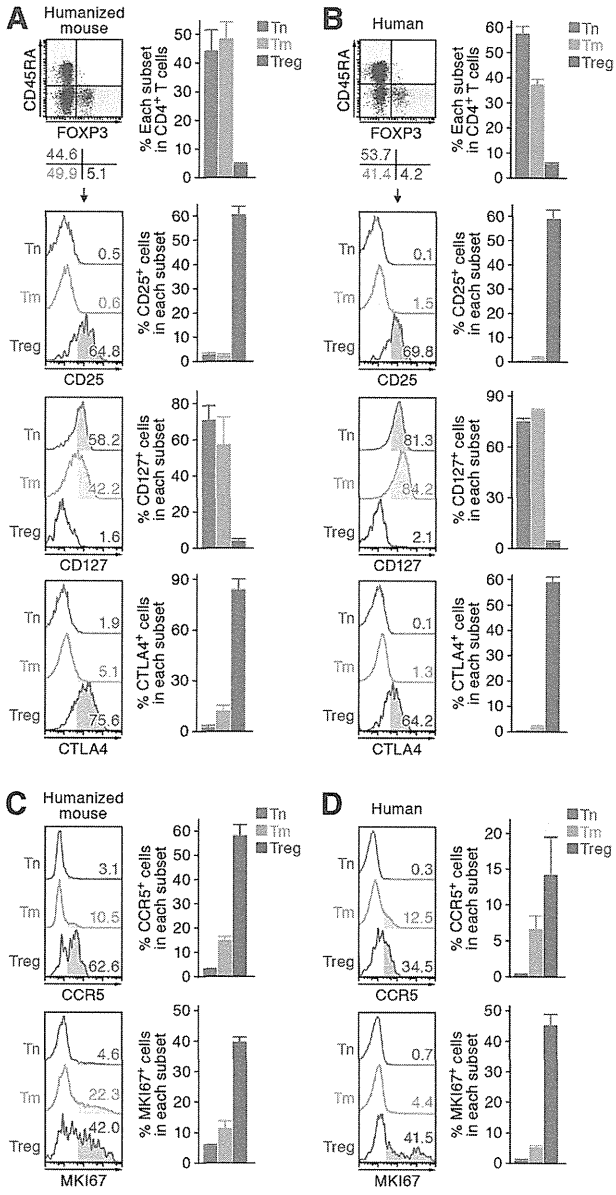

Figure 1. Comparison of the profile of $CD4^+$ T cell subsets between human and humanized mouse. Human $CD4^+$ T cells isolated from the spleen of humanized mice (A and C, n = 8) and the PB of HIV seronegative humans (B and D, n = 6) and were classified into Tn ($CD45^+$ $CD3^+$ $CD4^+$ $CD45RA^+$ $FOXP3^-$ cells), Tm ($CD45^+$ $CD3^+$ $CD4^+$ $CD45RA^-$ $FOXP3^-$ cells), and Treg ($CD45^+$ $CD3^+$ $CD4^+$ $CD45RA^-$ $FOXP3^+$ cells) by flow cytometry. Representative dot plots and histograms are shown on the left panels. The percentage of each subset in $CD4^+$ T cells (A and B, top) and the percentages of the cells positive for CD25, CD127, CTLA4, CCR5, and MKI67 in each subset are respectively shown on the right panels. In the left panels, the numbers under the dot plots (A and B, top) indicate the percentage of the cells in each quadrant, and the numbers in each histogram indicate the positivity. Data represent mean ± SEM.

doi:10.1371/journal.ppat.1003812.g001

associated protein 4 (CTLA4; also known as CD152) in humanized mice (Figure 1A) were similar to those in humans (Figure 1B). Since the suppressive function of the Tregs differentiated in humanized mouse models has been demonstrated previously [26–29], our results strongly suggest that the majority of

FOXP3$^+$ CD4$^+$ T cell population in our humanized mouse model is Tregs. Moreover, the expression level of CCR5, an HIV-1 coreceptor, was higher on Tregs than on Tms and Tns in both humans and humanized mice (Figure 1C and 1D). Furthermore, in line with previous studies reporting that Tregs actively proliferate *in vivo* [9–11], the percentage of the cells positive for MKI67 antigen identified by monoclonal antibody Ki-67 (MKI67; also known as Ki67) in Tregs of humans and humanized mice was significantly higher than those in Tms and Tns (Figure 1C and 1D). These results indicate that Tregs in humans and humanized mice are more actively cycling than Tns and Tms. Altogether, these results suggested that the profile and characteristics of CD4$^+$ T cell subsets in humanized mice mirror those in healthy humans.

To investigate the dynamics of each CD4$^+$ T cell subset after HIV-1 infection, 40 humanized mice were infected with a primary R5 HIV-1 isolate, strain JR-CSF [30]. As observed in HIV-1-infected individuals [15–17] and SIV-infected monkeys [18–20], we found that Tregs were preferentially and significantly decreased in the peripheral blood (PB) (Figure 2A and 2B) and the spleen (Figure 2C and 2D) of HIV-1-infected humanized mice until 21 days postinfection (dpi). However, because we have previously observed that surface CD4 molecules on HIV-1-infected cells in humanized mice are downregulated [21,23], we evaluated whether this was the case in Tregs. Results showed that Tregs were positive for surface CD4 (i.e., CD4$^-$ FOXP3$^+$ cells were absent) (Figure S1), indicating that the disappearance of Tregs during the acute phase of infection was not due to surface CD4 down-regulation, but rather to depletion by HIV-1 infection. Since CCR5 is highly expressed on Tregs (Figure 1C and 1D), we further assessed the level of CCR5$^+$ CD4$^+$ T cells in R5 HIV-1-infected humanized mice. As shown in Figure 2E, we observed zthat the percentage of CCR5$^+$ cells in the splenic CD4$^+$ T cells of R5 HIV-1-infected mice was significantly lower than that of mock-infected mice (Figure 2E). These findings suggest that R5 HIV-1 infection induces severe depletion of CCR5$^+$ CD4$^+$ T cells including Tregs during acute infection.

It is well known that Tregs have the potential to suppress immune activation *in vivo*, and that the depletion of Tregs induces aberrant immune activation [7]. To address this possibility in HIV-1-infected humanized mice, we assessed the immune activation status at 21 dpi by staining with CD38, an activation marker [31,32]. As shown in Figure 2F, the expression level of CD38 on memory CD8$^+$ T cells in the spleen of HIV-1-infected mice was significantly higher than that of mock-infected mice.

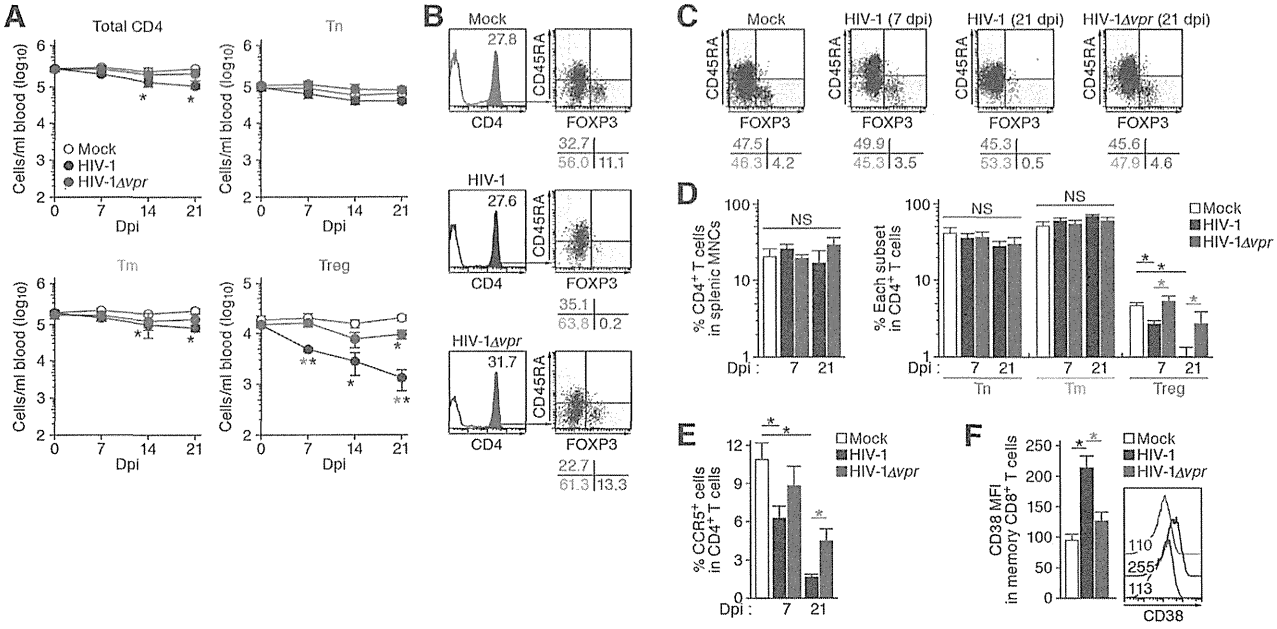

Figure 2. Dynamics of human CD4$^+$ T cell subsets in humanized mice infected with R5 WT and *vpr*-deficient HIV-1. (A and B) Longitudinal analyses of the dynamics of human CD4$^+$ T cell subsets in the PB of infected humanized mice. The numbers of total CD4$^+$ T cells (CD45$^+$ CD3$^+$ CD4$^+$ cells), Tns (CD45$^+$ CD3$^+$ CD4$^+$ CD45RA$^+$ FOXP3$^-$ cells), Tms (CD45$^+$ CD3$^+$ CD4$^+$ CD45RA$^-$ FOXP3$^-$ cells), and Tregs (CD45$^+$ CD3$^+$ CD4$^+$ CD45RA$^-$ FOXP3$^+$ cells) in the PB of R5 WT HIV-1-infected mice (n = 8), R5 *vpr*-deficient HIV-1-infected mice (n = 8), and mock-infected mice (n = 12) were routinely quantified by flow cytometry and hematocytometry. Summarized results (A) and representative dot plots at 21 dpi (B) are shown, respectively. In panel B, the numbers in the histogram indicate the percentage of CD4$^+$ cells in CD45$^+$ cells, and the numbers under the dot plots indicate the percentage of the cells in each quadrant. (C and D) Cytopathic effect of WT and *vpr*-deficient HIV-1 in the spleen of humanized mice. The percentages of total CD4$^+$ T cells, Tns, Tms, and Tregs in the splenic MNCs of WT HIV-1-infected mice (7 dpi, n = 19; 21 dpi, n = 8), *vpr*-deficient HIV-1-infected mice (7 dpi, n = 10; 21 dpi, n = 7), and mock-infected mice (n = 12) were routinely quantified by flow cytometry. Representative dot plots (C) and summarized results (D) are shown, respectively. In panel C, the numbers under the dot plots indicate the percentage of the cells in each quadrant. (E) The level of CCR5-expressing CD4$^+$ T cells in infected humanized mice. The percentage of CCR5$^+$ cells in the splenic CD4$^+$ T cells of WT HIV-1-infected mice (7 dpi, n = 8; 21 dpi, n = 6), *vpr*-deficient HIV-1-infected mice (7 dpi, n = 8; 21 dpi, n = 6), and mock-infected mice (n = 8) was analyzed by flow cytometry. (F) The level of immune activation in infected humanized mice. The MFI of CD38 in memory CD8$^+$ T cells (CD45$^+$ CD3$^+$ CD8$^+$ CD45RA$^-$ cells) in the spleen of WT HIV-1-infected mice (n = 5), *vpr*-deficient HIV-1-infected mice (n = 5), and mock-infected mice (n = 5) at 21 dpi was analyzed by flow cytometry. Representative histograms are shown on the right panel, and the numbers in the histogram indicate the MFI values. Statistical difference was determined by Welch's *t* test, and statistically significant differences ($P<0.05$) are shown as follows: mock versus WT HIV-1, black asterisk; mock versus HIV-1*Δvpr*, blue asterisk; and WT HIV-1 versus HIV-1*Δvpr*, red asterisk. NS, no statistical significance. Data represent mean ± SEM.

doi:10.1371/journal.ppat.1003812.g002

These results suggested that HIV-1 infection decreased Tregs in humanized mice and resulted in immune activation.

Vpr depletes Tregs and enhances HIV-1 propagation in a coreceptor-dependent manner

As described in Introduction section, Vpr is pleiotropic and is known to induce cell cycle arrest at the G_2 phase and apoptosis [1]. Since Tregs are highly proliferative *in vivo* (Figure 1), which is consistent with previous reports [9–11], we hypothesized that Tregs are highly susceptible to Vpr-mediated G_2 arrest. To test this hypothesis, 32 humanized mice were infected with R5 *vpr*-deficient HIV-1 (HIV-1*Δvpr*; strain JR-CSF) [33]. Although the infectivities of R5 WT HIV-1 and R5 HIV-1*Δvpr* were comparable *in vitro* (Figure S2), the level of viral load in the plasma of HIV-1*Δvpr*-infected mice at 4 and 7 dpi was significantly lower than that of WT HIV-1-infected mice (Figure 3A). These results suggested that HIV-1*Δvpr* is less replicative than WT HIV-1 during initial stage of infection in humanized mice. We also investigated the dynamics of $CD4^+$ T cells in HIV-1*Δvpr*-infected mice and found that the acute and severe depletion of Tregs after virus challenge was not observed in the PB (Figure 2A and 2B) and the spleen (Figure 2C and 2D). In addition, the level of $CCR5^+$ $CD4^+$ T cells in the spleen of HIV-1*Δvpr*-infected mice was significantly higher than that of WT HIV-1-infected mice (Figure 2E). Moreover, the immune activation, which was observed in WT HIV-1-infected mice, was not detected in HIV-1*Δvpr*-infected mice (Figure 2F). These findings suggested that Vpr enhances virus dissemination and induces Treg depletion leading to immune activation in humanized mice.

To address the association of Vpr with the rapid HIV-1 expansion *in vivo*, we next assessed the distribution of HIV-1-infected cells during acute infection (i.e., 7 dpi). As shown in Figure 3B, the percentage of the cells positive for p24, an HIV-1 antigen, in splenic $CD3^+$ $CD8^-$ cells of WT HIV-1-infected mice was comparable to that of HIV-1*Δvpr*-infected mice. We then examined the proportion of $p24^+$ cells in each $CD4^+$ T cell subset and found that Tregs were more positive for p24 than Tm and Tn in both WT HIV-1-infected and HIV-1*Δvpr*-infected mice (Figure 3C, left and right panels). In addition, we demonstrated that the percentage of $p24^+$ Tregs in WT HIV-1-infected mice was significantly higher than that in HIV-1*Δvpr*-infected mice (Figure 3C, left and right panels). Moreover, in WT HIV-1 but not in HIV-1*Δvpr*-infected mice, the mean fluorescent intensity (MFI) of p24, which reflects the expression level of viral proteins in infected cells, was significantly higher in Tregs than in Tns and Tms (Figure 3C, middle and right panels). Taken together, these results suggested that Tregs were highly susceptible to HIV-1 infection and produced large amounts of the virus with Vpr responsible for augmenting this production.

These findings raised the possibility that the preferential HIV-1 infection in Tregs was due to their high CCR5 expression (Figure 1C and 1D). To demonstrate this possibility, we assessed the expression level of CXCR4, another coreceptor for HIV-1, in each $CD4^+$ T cell subset. In both humans and humanized mice, we found that CXCR4 was broadly expressed in all $CD4^+$ T cell subsets and was highly expressed on Tns than Tms and Tregs (Figure 4A and 4B). Then, 13 humanized mice were infected with an X4 WT HIV-1 (strain NL4-3) [34], while 11 humanized mice were infected with an X4 HIV-1*Δvpr* (strain NL4-3) [2]. The infectivities of X4 WT HIV-1 and X4 HIV-1*Δvpr* were comparable *in vitro* (Figure S3). In contrast to the observations in R5 HIV-1-infected humanized mice (Figure 3A), the viral load of X4 WT HIV-1 and was comparable to that of X4 *vpr*-deficient HIV-1 (Figure 4C). In addition, the depletion of Tregs during the acute phase of infection, which was found in R5 HIV-1-infected mice (Figure 2A–2D), was not observed in the PB (Figure 4D) and the spleen (Figure 4E and 4F) of X4 WT HIV-1-infected mice. Furthermore, we did not observe the immune activation in X4 HIV-1-infected mice during acute infection (Figure 4G). Taken together, these findings strongly suggest that the preferential HIV-1 infection and the Treg depletion leading to immune activation during acute infection are dependent on the coreceptor usage of HIV-1.

Vpr induces a significant level of G_2 cell cycle arrest in infected Tregs

Extensive *in vitro* studies have reported that Vpr can cause cell cycle arrest at the G_2 phase [1]. To investigate the cell cycle condition of R5 HIV-1-infected cells in humanized mice at 7 dpi, cellular DNA content was quantified by Hoechst staining. Although the percentages of p24-negative cells at the G_2M phase in the spleen of WT HIV-1-infected and HIV-1*Δvpr*-infected cells were similar to those of mock-infected mice, a significant level of p24-positive cells at the G_2M phase in both WT HIV-1-infected and HIV-1*Δvpr*-infected mice were detected (Figure 5A). Moreover, we found that the percentage of $p24^+$

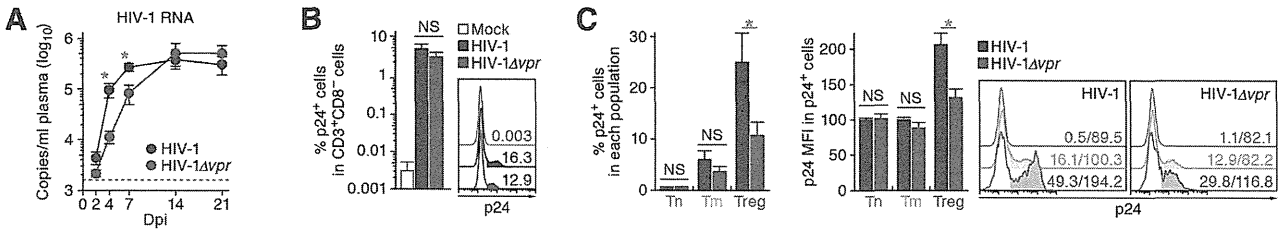

Figure 3. Dynamics of R5 WT and *vpr*-deficient HIV-1 infection in humanized mice. (A) Viral load in infected humanized mice. The amounts of viral RNA in the plasma of R5 WT HIV-1-infected mice (n = 30) and R5 *vpr*-deficient HIV-1-infected mice (n = 23) were routinely quantified. The horizontal broken line indicates the detection limit of the assay (1,600 copies/ml). (B and C) Infected cells in humanized mice. HIV-1-infected cells in the spleen of R5 WT HIV-1-infected mice (n = 19), R5 *vpr*-deficient HIV-1-infected mice (n = 10), and mock-infected mice (n = 10) at 7 dpi were analyzed by flow cytometry using an anti-HIV-1 p24 antibody. The percentages of $p24^+$ cells in $CD3^+$ $CD8^-$ cells (B) and in each $CD4^+$ T cell subset (C, left panel), and the MFI of p24 in $p24^+$ cells of each $CD4^+$ T cell subset (C, middle panel) are shown. Representative histograms are shown on the right panel. In panel B, the numbers in the histogram indicate the positivity. In panel C, the numbers in the histogram indicate the percentage of positive cells (left) and MFI values (right). Statistical difference was determined by Welch's *t* test, and statistically significant differences between WT HIV-1 versus HIV-1*Δvpr* ($P<0.05$) are shown with red asterisks. NS, no statistical significance. Data represent mean ± SEM.
doi:10.1371/journal.ppat.1003812.g003

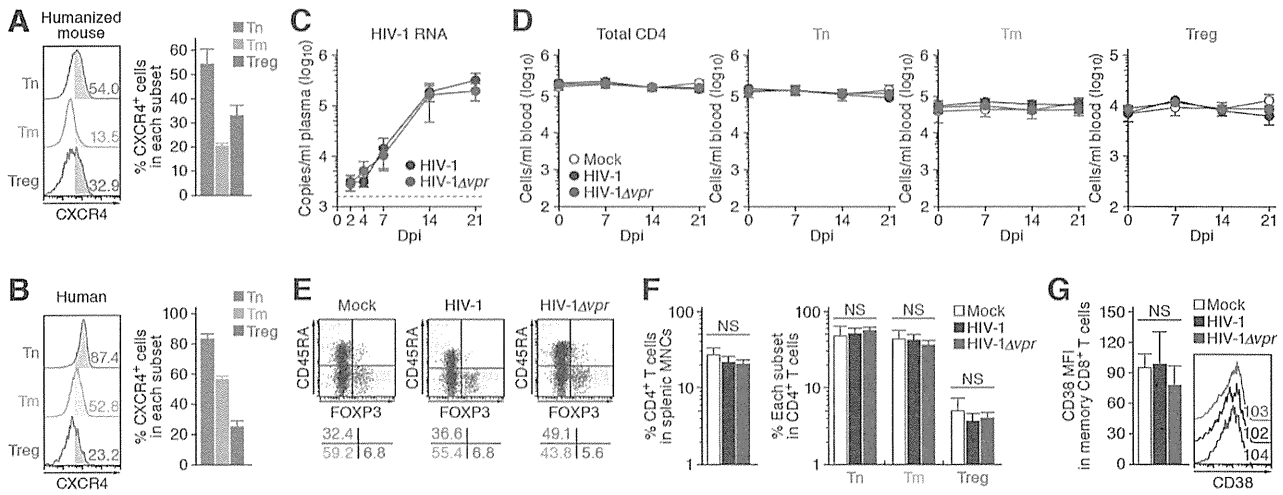

Figure 4. Dynamics of X4 WT and *vpr*-deficient HIV-1 infection in humanized mice. (A and B) CXCR4 expression on $CD4^+$ T cell subsets in human and humanized mouse. Human $CD4^+$ T cells isolated from the spleen of humanized mice (A, n = 8) and the PB of HIV seronegative humans (B, n = 6) were classified into Tn, Tm, and Treg as described in the legend of Figure 1. Representative dot plots and histograms are shown on the left, and the percentages of $CXCR4^+$ cells in each subset are shown on the right. In the left panels, the numbers in each histogram indicate the positivity. (C) Viral load in infected humanized mice. The amounts of viral RNA in the plasma of X4 WT HIV-1-infected mice (n = 13) and X4 *vpr*-deficient HIV-1-infected mice (n = 11) were routinely quantified. The horizontal broken line indicates the detection limit of the assay (1,600 copies/ml). (D) Longitudinal analyses of the dynamics of human $CD4^+$ T cell subsets in the PB of infected humanized mice. The numbers of total $CD4^+$ T cells, Tns, Tms, and Tregs in the PB of WT HIV-1-infected mice (n = 9), *vpr*-deficient HIV-1-infected mice (n = 9), and mock-infected mice (n = 8) were routinely quantified by flow cytometry and hematocytometry. (E and F) Cytopathic effect of WT and *vpr*-deficient HIV-1 in the spleen of humanized mice. The percentages of total $CD4^+$ T cells, Tns, Tms, and Tregs in the splenic MNCs of WT HIV-1-infected mice (n = 8), *vpr*-deficient HIV-1-infected mice (n = 8), and mock-infected mice (n = 8) at 21 dpi were routinely quantified by flow cytometry. Representative dot plots (E) and summarized results (F) are shown, respectively. In panel E, the numbers on the right of the dot plots indicate the percentage of the cells in each quadrant. (G) The level of immune activation in infected humanized mice. The MFI of CD38 in memory $CD8^+$ T cells in the spleen of WT HIV-1-infected mice (n = 5), *vpr*-deficient HIV-1-infected mice (n = 5), and mock-infected mice (n = 5) at 21 dpi was analyzed by flow cytometry. Representative histograms are shown on the right panel, and the numbers in the histogram indicate the MFI values. NS, no statistical significance. Data represent mean ± SEM.
doi:10.1371/journal.ppat.1003812.g004

cells at the G_2M phase in WT HIV-1-infected mice was significantly higher than that in HIV-1*Δvpr*-infected mice (Figure 5A), suggesting that Vpr expressed in infected cells induced G_2 cell cycle arrest *in vivo*.

We next analyzed the level of G_2 arrest in each $CD4^+$ T cell subset. Since $p24^+$ cells were faintly detected in the Tn subset (Figure 3C; 0.33±0.1% for WT HIV-1, 0.35±0.1% for HIV-1*Δvpr*), we focused on Tms and Tregs. In both subsets, the percentages of G_2M cells in $p24^-$ cells of WT HIV-1-infected and HIV-1*Δvpr*-infected mice were similar to those of mock-infected mice (Figure 5B). In contrast, we detected a significant level of $p24^+$ cells at the G_2M phase in Tms and Tregs (Figure 5B). Of note, the percentage of G_2M cells in $p24^+$ Tregs of WT HIV-1-infected mice reached a maximum of 37.1±2.8% and was significantly higher than that of HIV-1*Δvpr*-infected mice (Figure 5B). These results suggested that the level of Vpr-mediated G_2 arrest was the highest in HIV-1-infected Tregs.

Since it has been suggested that the G_2 arrest in HIV-1-infected cells results in the augmentation of virus production [3,35], we next focused on the relationship between the HIV-1 production potential and cell cycle condition in Tms and Tregs. Figure 5C illustrated that G_2M cells displayed higher percentages of p24-positive cells than G_0G_1 cells in both Tm and Treg. Surprisingly, 74.1±5.4% of Tregs at the G_2M phase in WT HIV-1-infected mice were positive for p24 (Figure 5C, left and right panels), and the p24 MFI in $p24^+$ Tregs at G_2M phase was highest (Figure 5C, middle and right panels). Taken together, these findings suggested that the majority of Tregs were infected with HIV-1 and arrested at the G_2 phase by Vpr, resulting in the augmentation of HIV-1 production during acute infection.

Vpr directly induces apoptosis in infected Tregs associated with G_2 cell cycle arrest

In addition to the augmentation of viral replication by Vpr, we also observed a severe depletion of Tregs in R5 WT HIV-1-infected humanized mice (Figure 2A–2D). It is known that Vpr can induce apoptosis through a caspase 3/8 (CASP3/8)-dependent pathway [1]. Therefore, we next analyzed the level of active CASP3, which is a direct inducer of apoptosis, in infected humanized mice. In the population of p24-negative cells, we found a significant increase of active $CASP3^+$ cells in WT HIV-1-infected mice (Figure 6A). Additionally, in both WT HIV-1-infected and HIV-1*Δvpr*-infected mice, the percentage of active CASP3 in $p24^+$ cells was significantly higher than that in $p24^-$ cells, yet the percentage of active CASP3 in $p24^+$ cells of WT HIV-1-infected cells was significantly higher than that of HIV-1*Δvpr*-infected mice (Figure 6A).

We then evaluated the magnitude of apoptosis in each $CD4^+$ T cell subset. As shown in Figure 6B, the percentage of active $CASP3^+$ cells in $p24^-$ Tms and Tregs of WT HIV-1-infected mice significantly increased when compared with those of mock-infected mice. On the other hand, the percentage of active $CASP3^+$ cells was significantly increased in $p24^+$ cells and was highest in $p24^+$ Tregs of WT HIV-1-infected mice (26.6±3.9%; Figure 6B), suggesting that Tregs are highly sensitive to Vpr-mediated apoptosis.

In addition to the apoptosis directly induced by Vpr, accumulating evidence has suggested a role for innate immune activation, including NK cells, in the $CD4^+$ T cell depletion after primary HIV-1 infection in individuals [36,37]. Also, it has been recently reported that Vpr upregulates the surface expression of some NK receptor ligands, such as UL16 binding protein 2

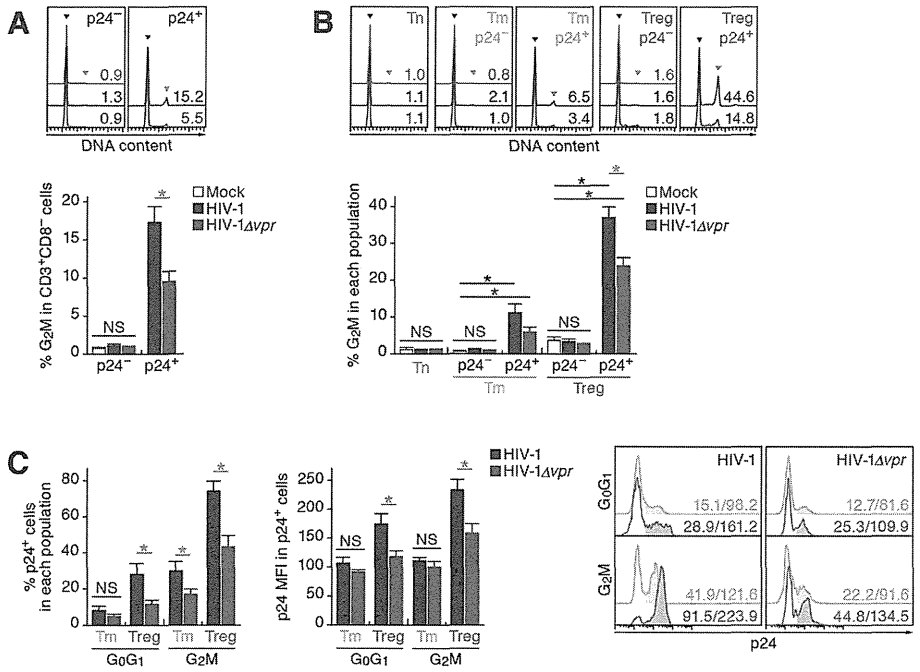

Figure 5. Effect of Vpr on G_2 cell cycle arrest in infected humanized mice. Splenic MNCs of WT HIV-1-infected mice (n = 12), *vpr*-deficient HIV-1-infected mice (n = 11), and mock-infected mice (n = 15) at 7 dpi were analyzed by flow cytometry using Hoechst33342 and an anti-HIV-1 p24 antibody. (A and B) The percentages of G_2M cells in $CD3^+$ $CD8^-$ cells (A) and in each population (B) are shown, respectively. Representative histograms are shown on the right panel. The black arrowhead indicates the peak of G_0G_1 cells, and the red arrowhead indicates the peak of G_2M cells. The numbers in the histogram indicate the percentage of G_2M cells in each population. (C) The percentage of $p24^+$ cells in each population (left) and the MFI of p24 in $p24^+$ cells of each population (middle). Representative histograms are respectively shown. The numbers in the histogram indicate the percentage of positive cells (left) and MFI values (right). Statistical differences were determined by Welch's *t* test, and statistically significant differences ($P<0.05$) are shown as follows: mock versus WT HIV-1, black asterisk; mock versus HIV-1*Δvpr*, blue asterisk; and WT HIV-1 versus HIV-1*Δvpr*, red asterisk. NS, no statistical significance. Data represent mean ± SEM.
doi:10.1371/journal.ppat.1003812.g005

(ULBP2), which leads to NK cell-dependent cell death [38,39]. These reports led to the hypothesis that Vpr upregulates the expression level of ULBP2 on HIV-1-infected Tregs and enhances NK cell-dependent cell death. To address this possibility, we assessed the expression level of ULBP2 in infected humanized mice. However, the expression level of ULBP2 on the surface of WT HIV-1-infected cells was comparable to those of HIV-1*Δvpr*-infected cells, uninfected cells, and the $CD4^+$ T cells in mock-infected mice (Figure S4). Taken together, these results suggested that the decrease of Tregs in R5 WT HIV-1-infected mice was not dependent on the NK cell-dependent cell death but due to Vpr expressed in infected cells.

In order to investigate the relationship between G_2 cell cycle arrest and apoptosis, both of which are mediated by Vpr, we performed p24 staining in combination with Hoechst and active CASP3 staining. In each $CD4^+$ T cell subset positive for p24, the percentage of active $CASP3^+$ cells at G_2M was significantly higher than that at the G_0G_1 phase (Figure 6C). Moreover, the percentage of active $CASP3^+$ cells was highest in $p24^+$ Tregs at G_2M in WT HIV-1-infected mice (35.9±5.4%; Figure 6C), strongly suggesting that Vpr-mediated apoptosis was most efficiently induced in infected Tregs arrested at the G_2 phase.

Treg depletion can trigger immune activation and augmented HIV-1 propagation *in vivo*

The aforementioned findings suggested that Vpr promotes R5 HIV-1 propagation during the acute phase of infection by exploiting proliferating $CCR5^+$ $CD4^+$ T cells including Tregs *in vivo*. In addition, Vpr is associated with the rapid decrease of Tregs, leading to immune activation. Since it is known that HIV-1 replicates more efficiently in activated $CD4^+$ T cells than non-activated $CD4^+$ T cells [40,41], our findings suggested that the immune activation induced by Vpr-mediated Treg depletion led to the augmented viral propagation *in vivo*. To address this possibility, denileukin diftitox (DD), which is known to specifically target and deplete Tregs, was intraperitoneally treated into humanized mice. As shown in Figure 7A and 7B, Tregs were specifically and significantly depleted by treatment with DD for 3 days, while the cell numbers of the other populations such as $CD45^+$ human white blood cells, total $CD4^+$ T cells, Tns, and Tms did not change significantly. We also found that the Treg depletion by DD induced immune activation and proliferation of splenic memory $CD8^+$ T cells (Figure 7C). Interestingly, the percentage of $MKI67^+$ cells in the Tms of DD-treated humanized mice was significantly higher than those in Tms and Tregs of untreated humanized mice (Figure 7D). In addition, the levels of CCR5 on Tms and Tns in DD-treated mice were significantly higher than that in untreated mice (Figure 7E), suggesting that the population size of proliferating $CCR5^+$ $CD4^+$ T cells in DD-treated humanized mice is greater than that in untreated humanized mice.

R5 WT and *vpr*-deficient HIV-1 (strain JR-CSF) were then inoculated into 13 DD-treated humanized mice, respectively. As shown in Figure 7F, the number of $CD4^+$ T cells, particularly Tms, in the PB of DD-treated uninfected mice gradually increased, while that those of DD-treated WT and *vpr*-deficient

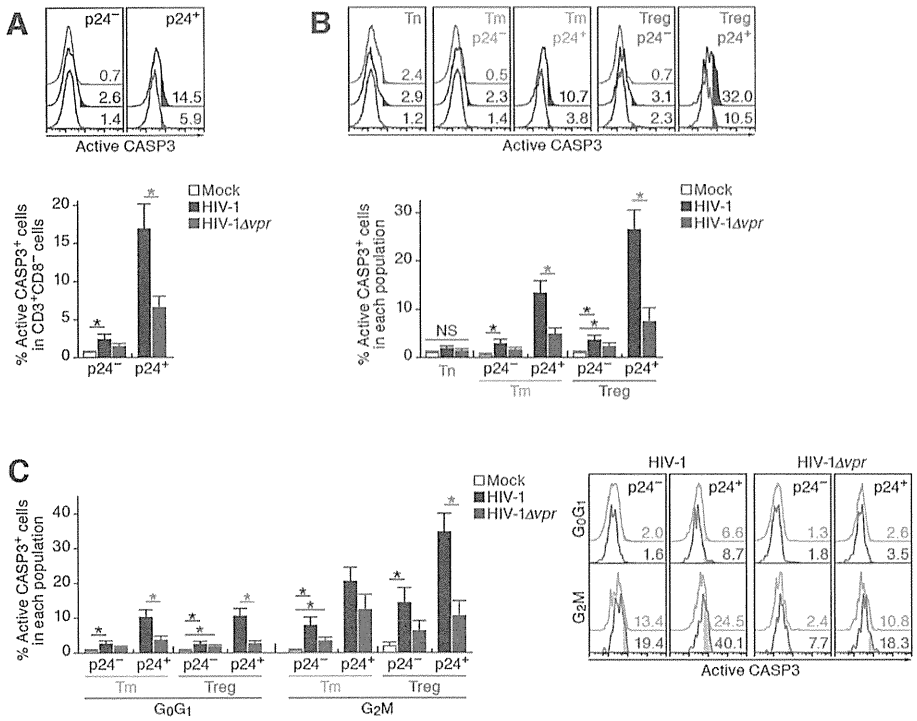

Figure 6. Effect of Vpr on apoptosis and its relevance in G_2 cell cycle arrest in infected humanized mice. Splenic MNCs of WT HIV-1-infected mice (n = 7), *vpr*-deficient HIV-1-infected mice (n = 7), and mock-infected mice (n = 9) at 7 dpi were analyzed by flow cytometry using anti-active CASP3 and anti-HIV-1 p24 antibodies without (A and B) or with (C) or Hoechst33342. (A and B) Effect of Vpr on apoptosis. The percentages of active CASP3$^+$ cells in CD3$^+$ CD8$^-$ cells (A) and in each population (B) are shown, respectively. Representative histograms are shown on the right panel. The numbers in the histogram indicate the percentage of active CASP3$^+$ cells in each population. (C) Relevance between G_2 arrest and apoptosis. The percentage of active CASP3$^+$ cells in each population is shown. Representative histograms are respectively shown. The numbers in the histogram indicate the percentage of active CASP3$^+$ cells in each population. Statistical differences were determined by Welch's *t* test, and statistically significant differences ($P<0.05$) are shown as follows: mock versus WT HIV-1, black asterisk; mock versus HIV-1*Δvpr*, blue asterisk; and WT HIV-1 versus HIV-1*Δvpr*, red asterisk. NS, no statistical significance. Data represent mean ± SEM.
doi:10.1371/journal.ppat.1003812.g006

HIV-1 infected mice severely decreased after 7 dpi. We also observed a gradual increase of memory CD8$^+$ T cells in the PB of DD-treated humanized mice regardless of HIV-1 infection (Figure S5). It was of particular importance that rapid and massive HIV-1 replication in DD-treated mice compared with untreated mice infected with either virus, and that the viral load in DD-treated WT HIV-1-infected mice was significantly higher than that in DD-treated HIV-1*Δvpr*-infected mice at 4 and 7 dpi (Figure 7G). Furthermore, the slope of virus growth in DD-treated WT HIV-1-infected mice was significantly higher than those of DD-treated HIV-1*Δvpr*-infected mice and untreated WT HIV-1-infected mice (Figure 7H). Taken together, these findings suggest that R5 HIV-1 massively propagates under an activated condition, and that Vpr enhances viral expansion in CCR5$^+$ proliferating CD4$^+$ T cell population.

Discussion

The fact that *vpr* is conserved in transmitted/founder viruses in infected individuals [42] may indicate its importance during the acute phase of HIV-1 propagation. However, even though there is abundant evidence of Vpr's roles in G_2 arrest and apoptosis *in vitro* [1,43,44], its impact on for HIV-1 replication *in vivo* remains unclear. In this study, we demonstrated that Vpr augments R5 HIV-1 propagation by exploiting proliferating CCR5$^+$ CD4$^+$ T cells including Tregs during acute infection. We also observed significant levels of Vpr-dependent G_2 arrest and apoptosis in R5 HIV-1-infected Tregs, which may result in the Treg depletion and subsequent immune activation. This is the first report to directly demonstrate that Vpr positively affects HIV-1 replication by taking advantage of Tregs *in vivo*.

A previous study has demonstrated that Tregs highly express CCR5, correlating with their high susceptibility to R5 HIV-1 *in vitro* [15]. Here, by using a humanized mouse model, we demonstrated that Tregs express higher level of CCR5 (Figure 1) and are highly susceptible to R5 HIV-1 infection *in vivo* (Figure 3). In addition, it is well known that HIV-1 replicates more efficiently in activated/proliferating cells than in non-activated cells [40,41]. Consistent with previous reports [9–11], we showed that Tregs are highly proliferative *in vivo* when compared with the other CD4$^+$ T cell subsets such as Tns and Tms (Figure 1). Therefore, it is reasonable to assume that R5 HIV-1 efficiently replicates in Tregs of humanized mice because of their higher CCR5 expression level and higher proliferating status. Moreover, in line with the previous observations that Vpr arrests the cell cycle of HIV-1-infected cells at G_2 phase where LTR-driven HIV-1 transcription is most active [3,35], we found that the MFI of p24, which reflects the expression level of viral proteins, in Tregs of WT HIV-1-infected mice was ~2-fold higher than that of HIV-1*Δvpr*-infected mice, while expression levels in Tns and Tms were comparable between WT and *vpr*-deficient HIV-1 (Figure 3C). Furthermore, we revealed that Vpr-dependent G_2

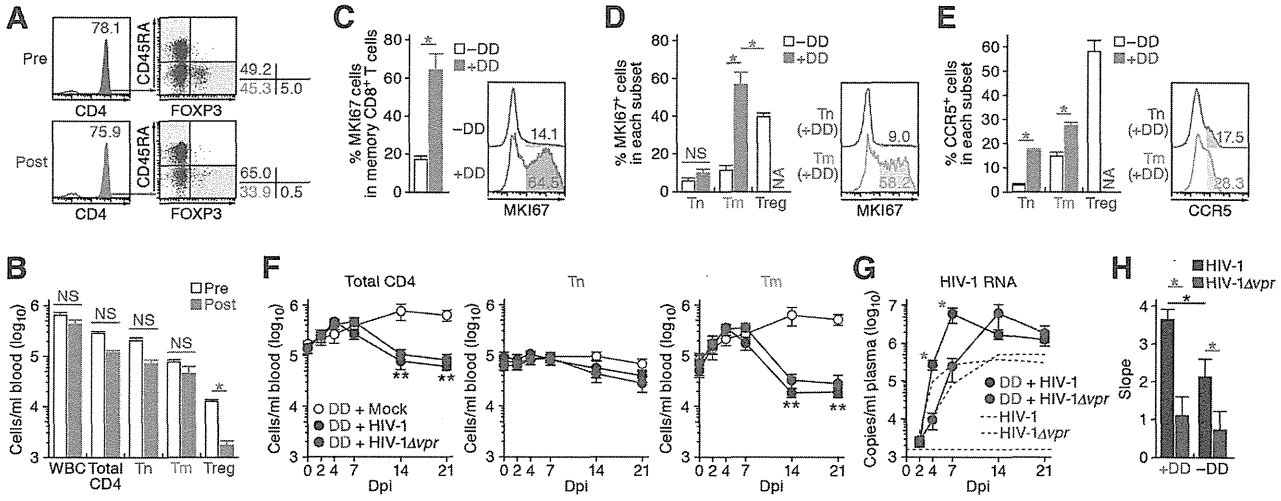

Figure 7. Augmentation of Vpr's effect and HIV-1 propagation by Treg depletion. (A to D) Evaluation of Treg depletion by treatment with DD. DD was administrated into humanized mice (n = 14) as described in Materials and Methods. (A and B) Specific depletion of Tregs by treatment with DD. The levels of human white blood cells (WBC; $CD45^+$ cells) and $CD4^+$ T cell subsets in PB of humanized mice before and after the DD treatment for 3 days were compared. Representatives (A) and the numbers of each human leukocytes in PB (B) are shown. In panel A, the numbers in the histogram indicate the percentage of $CD4^+$ cells in $CD45^+$ $CD3^+$ cells, and the numbers on the right of the dot plots indicate the percentage of the cells in each quadrant. (C and D) Immune activation by treatment with DD. The percentages of $MKI67^+$ cells in memory $CD8^+$ T cells (C) and in each $CD4^+$ T cell subset (D) in the spleen of humanized mice treated with (n = 5) or without (n = 8) DD for 7 days are shown, respectively. (E) Up-regulation of CCR5 expression by DD treatment. The percentage of $CCR5^+$ cells in each $CD4^+$ T cell subset in the spleen of humanized mice treated with (n = 5) or without (n = 8) DD for 7 days is shown. In panels C to E, the numbers in the histogram indicate positivity. (F to H) Dynamics of HIV-1 infection in DD-treated humanized mice. (F) The numbers of peripheral $CD4^+$ T cells, Tns, Tms, and Tregs (F) and the amounts of viral RNA in the plasma (G) of R5 WT HIV-1-infected DD-treated mice (n = 13), R5 *vpr*-deficient HIV-1-infected DD-treated mice (n = 13), and mock-infected DD-treated mice (n = 8) were routinely quantified as described in the legends of Figure 2A and 3A, respectively. In panel G, the broken black and blue lines indicate the averages of WT HIV-1-infected mice (n = 30) and *vpr*-deficient HIV-1-infected mice (n = 23) without DD treatment, which corresponds to the results shown in Figure 3A. The horizontal broken line indicates the detection limit of the assay (1,600 copies/ml). (H) Kinetics of viral expansion. The slopes of the amounts of viral RNA in the plasma of WT HIV-1-infected DD-treated mice (n = 13), *vpr*-deficient HIV-1-infected DD-treated mice (n = 13), WT HIV-1-infected mice (n = 30) and *vpr*-deficient HIV-1-infected mice (n = 23) until 7 dpi are shown. Statistical difference was determined by Welch's *t* test. In panels B to E, statistically significant differences ($P<0.05$) are indicated by red asterisks. In panels F and G, statistically significant differences ($P<0.05$) are shown as follows: mock versus WT HIV-1, black asterisk; mock versus HIV-1*Δvpr*, blue asterisk; and WT HIV-1 versus HIV-1*Δvpr*, red asterisk. In panel H, statistically significant differences ($P<0.05$) are shown as follows: with and without DD treatment, black asterisk; and WT HIV-1 versus HIV-1*Δvpr*, red asterisk. NS, no statistical significance. Data represent mean ± SEM. NA, not analyzed.
doi:10.1371/journal.ppat.1003812.g007

cell cycle arrest was efficiently occurred in infected Tregs (Figure 5B), and that both the percentage $p24^+$ cells and the p24 MFI was highest in WT HIV-1-infected Tregs at G_2 phase (Figure 5C). Taken together, these findings strongly suggest that Vpr promotes R5 HIV-1 replication during acute infection by increasing the viral production in Tregs.

In contrast to the findings in R5 HIV-1-infected humanized mouse model, we observed neither the acceleration of virus replication by Vpr during the acute phase of HIV-1 infection (Figure 4C), nor the Treg depletion (Figure 4D–4F), nor subsequent immune activation (Figure 4G) in X4 HIV-1-infected humanized mice. In Tregs, CCR5 is predominantly expressed (Figure 1C and 1D), whereas CXCR4 is broadly expressed in all $CD4^+$ T cell subsets (Figure 4A and 4B), which is consistent with previous findings [15,28]. Therefore, these results suggest that the Vpr-dependent augmentation of HIV-1 replication during acute infection is dependent on viral tropism and is restricted to R5 HIV-1. Regarding HIV-1 tropism, it is of particular importance that R5 HIV-1 is the major clinical isolates from patients, along with transmitted/founder viruses [42,45,46], while X4 HIV-1 occasionally emerges during the onset of AIDS [47,48]. Therefore, the findings in R5 HIV-1-infected humanized mice more properly reflect those in patients than those in X4 HIV-1-infected mice, and the role of Vpr in R5 HIV-1-infected humanized mice is physiologically more relevant.

The concept that Vpr augments R5 HIV-1 replication by utilizing proliferating $CCR5^+$ $CD4^+$ T cells is further supported by the DD treatment experiments (Figure 7): the human leukocytes including Tms in the mice treated with DD were highly proliferative and the Tms in DD-treated mice expressed higher level of CCR5. Moreover, R5 HIV-1 propagated more efficiently when compared with the untreated mice. Interestingly, it has been reported that Vpr enhances HIV-1 LTR-driven transcription in cycling $CD4^+$ T cells but not in non-cycling cells [3]. Taken together, these findings suggest that Vpr-dependent promotion of R5 HIV-1 production during acute infection is attributed to the target cell tropism of HIV-1 and the activated/proliferative status of the target cells.

There is a longstanding dogma that the immune activation caused by HIV-1/SIV infection closely associates with the disease progression [49]. Regarding the triggering of immune activation, previous studies have suggested that the immune activation in HIV-1-infected individuals and SIV-infected monkeys can be caused by (1) massive infection and loss of $CD4^+$ T cells [50,51]; (2) inflammatory cytokines [52,53]; and (3) microbial translocation from the luminal intestinal tract [54]. In this study, Treg depletion and immune activation were observed in R5 but not X4 HIV-1-infected humanized mice (Figure 2 and 4). These findings are consistent with previous observations in HIV-1-infected patients [15–17], SIV-infected monkeys [18–20], and a CCR5/CXCR4

dual-tropic HIV-1-infected humanized mouse model [28]. Particularly noteworthy is that *vpr*-deficient HIV-1-infected humanized mice showed neither Treg depletion nor immune activation. These findings raise a possibility that Vpr is associated with the induction of immune activation by depleting Tregs. Since the physiological role of Tregs *in vivo* is to suppress excessive immune activation [7], it is conceivable that Vpr-mediated Treg depletion can be one of the triggers for immune activation in HIV-1-infected individuals. However, the mechanism of the immune activation by HIV-1/SIV infection still remains unsolved for more than two decades of intense research, and there are lines of other possibilities such as the activation of dendritic cells/macrophages due to higher number of cell death [55–57] and the actual depletion of myeloid-derived suppressor cells [58,59] by direct or indirect virus infection. Although our results suggest that Vpr is associated with the acute Treg depletion and subsequent immune activation in R5 HIV-1-infected humanized mice, further investigations is necessary to elucidate the mechanisms of the immune activation by HIV-1/SIV infection.

In DD-treated humanized mice, we observed the activation/proliferation (Figure 7C) and the expansion (Figure S5) of memory $CD8^+$ T cells. As a previous report using R5 HIV-1-infected humanized mice showed that the depletion of $CD8^+$ T cells accelerates HIV-1 replication [60], these findings raise a possibility that the expanded memory $CD8^+$ T cells restrict HIV-1 replication in DD-treated humanized mice. However, the previous study [60] depleted $CD8^+$ T cells in R5 HIV-1-infected humanized mice during chronic infection (i.e, 5–7 weeks postinfection) and observed the increase of virus growth 2 weeks after $CD8^+$ T cell depletion. On the other hand, although the increase of memory $CD8^+$ T cells was observed in DD-treated humanized mice after 4 or 7 dpi (Figure S5), here we particularly focused on the dynamics of HIV-1 infection during the acute phase (i.e., until 7 dpi) and observed a sharp increase of HIV-1 replication in DD-treated mice prior to the expansion of memory $CD8^+$ T cells (Figure 7G). Moreover, the activation and expansion of $CD8^+$ T cells were detected in DD-treated humanized mice regardless of HIV-1 infection, strongly suggesting that this $CD8^+$ T cell expansion is not triggered by HIV-1 infection but by the DD-mediated Treg depletion. Furthermore, although the expansion of memory $CD8^+$ T cells during chronic infection has been observed in certain HIV-1-infected human HSC-transplanted humanized mouse models [61–63] including ours [25], it is controversial whether or not the human $CD8^+$ T cells differentiated in human HSC-transplanted humanized mouse models possess the potential to efficiently elicit acquired immune responses against pathogens including HIV-1 [64–66]. These findings suggest that the expanded $CD8^+$ T cells in DD-treated humanized mice have smaller effect on the virus growth during the acute phase of HIV-1 infection.

Soluble Vpr proteins are secreted from infected cells and can be detected in patient sera [67,68]. In p24-negative cells of WT HIV-1-infected mice, we found a significant level of apoptosis (Figure 6A and 6B), while G_2 arrest was not observed (Figure 5A and 5B). These results suggest that soluble Vpr can trigger apoptosis but not G_2 arrest in bystander cells. In fact, it was reported that the Vpr expressed in HIV-1-infected cells robustly induce both G_2 arrest and apoptosis, while soluble Vpr secreted from HIV-1-infected cells can induce apoptosis but not G_2 arrest [69]. However, in addition to WT HIV-1-infected cells, G_2 arrest was also partially observed in HIV-1*Δvpr*-infected cells (Figure 5A and 5B). In this regard, it has been reported that another accessory protein of HIV-1, Vif, is also able to cause G_2 arrest in a Vpr-independent manner [70–72], strongly suggesting that the G_2 arrest in HIV-1*Δvpr*-infected cells is induced by Vif. Although the significance of functional redundancy of Vpr and Vif for G_2 arrest remains unclear, further studies using humanized mice will reveal their impact.

In summary, we demonstrated for the first time that one of the major roles of Vpr in HIV-1 infection and pathogenesis is to enhance R5 HIV-1 propagation by exploiting proliferating $CCR5^+$ $CD4^+$ T cells including Tregs during acute infection, which can subsequently induce immune activation. Our findings suggest that the action of Vpr *in vivo* may provide HIV-1 with an optical condition to replicate and facilitate HIV-1 expansion *in vivo*.

Materials and Methods

Ethics statement

All procedures including animal studies were conducted following the guidelines for the Care and Use of Laboratory Animals of the Ministry of Education, Culture, Sports, Science and Technology, Japan. These studies were approved by the Institutional Animal Care and Use Committees (IACUC)/ethics committee of Kyoto University (protocol number D13–25). All protocols involving human subjects were reviewed and approved by the Kyoto University institutional review board. Informed written consent from human subjects was obtained in this study.

Humanized mice

NOD.Cg-*Prkdc*^{scid} *Il2rg*^{tm1Sug}/*Jic* (NOD/SCID *Il2rg*$^{-/-}$) mice [73] were obtained from the Central Institute for Experimental Animals (Kawasaki, Kanagawa, Japan). The mice were maintained under specific-pathogen-free conditions and were handled in accordance with the regulations of the IACUC/ethics committee of Kyoto University. Human $CD34^+$ HSCs were isolated from human fetal liver as described previously [74]. The humanized mouse (NOG-hCD34 mouse) was constructed as previously described [21–24]. Briefly, 164 newborn (aged 0 to 2 days) NOG mice from 38 litters were irradiated with X-ray (10 cGy per mouse) by an RX-650 X-ray cabinet system (Faxitron X-ray Corporation) and were then intrahepatically injected with the obtained human fetal liver-derived $CD34^+$ cells (7.5×10^4 to 25×10^4 cells). A list of the humanized mice used in this study is summarized in Table S1.

Virus preparation and infection

Virus solutions of R5 WT HIV-$1_{JR\text{-}CSF}$ [30], R5 *vpr*-deficient HIV-$1_{JR\text{-}CSF}$ [33], X4 WT HIV-$1_{NL4\text{-}3}$ [34], and X4 *vpr*-deficient HIV-$1_{NL4\text{-}3}$ [2] were prepared and titrated as previously described [23]. Virus solutions of 10^5 50% tissue culture infectious doses ($TCID_{50}$) were intraperitoneally inoculated into NOG-hCD34 mice. RPMI 1640 was used for mock infection.

HIV-1 RNA quantification, TZM-bl assay, and western blotting

The amount of HIV-1 RNA in plasma was quantified by Bio Medical Laboratories, Inc. TZM-bl assay and Western blotting were performed as previously described [22,23]. For Western blotting, mouse anti-Vpr antibody (clone 8D1) [68] and goat anti-p24 antiserum (ViroStat) were used.

PB collection and isolation of splenic mononuclear cells

PB and plasma were routinely collected as previously described [21–24]. Splenic human mononuclear cells (MNCs) were isolated as previously described [22–24].

Flow cytometry and hematocytometry

Flow cytometry was performed with FACSCanto (BD Biosceiences) as previously described [21–24]. Hematocytometry was performed with Celltac alpha MEK-6450 (Nihon Kohden Co) as previously described [23,24]. Briefly, 10 μl of the PB of humanized mice were used for hematometry, and the number of MNCs per microliter was measured. The antibodies used in flow cytometry analysis are listed in Table S2. For cell cycle analysis, cellular DNA was stained with Hoechst33342 (Invitrogen) as previously described [21], and DNA contents were analyzed by using ModFit LT software (Verify software house) according to the manufacture's protocol and as previously reported [72]. For the measurement of the level of apoptosis, anti-active CASP3 antibody conjugated with PE (BD Biosciences; Table S2) was used according to the manufacture's procedure.

Denileukin diftitox treatment for Treg depletion

Denileukin diftitox (DD; IL-2 conjugated with diphtheria toxin) were purchased from Ligand Pharma, Co. For Treg depletion in humanized mice, DD (400 μg/200 μl in PBS) were intraperitoneally treated once per day. For HIV-1 infection following DD treatment, the humanized mice treated with DD for 3 days were intraperitoneally inoculated with virus solutions of 10^5 $TCID_{50}$. RPMI 1640 was used as the mock infection. To maintain Treg depletion following virus inoculation, DD was intraperitoneally treated once per day.

Statistical analyses

Data were expressed as averages with SEMs. Significant differences ($P<0.05$) were determined by Welch's t test or Student's t test.

Accession numbers

SwissProt (http://www.uniprot.org/) or GenBank (http://www.ncbi.nlm.nih.gov/genbank) accession numbers for the proteins mentioned in the text are as follows: CD3 (P07766); CD4 (P01730); CD8 (NP_001759.3); CD25 (NP_000408.1); CD38 (P28907); CD45 (NP_002829.3); CD45RA (P08575); CD127 (P16871); CASP3 (P42574); CCR5 (P51681); CXCR4 (P61073); CTLA4 (P16410); FOXP3 (Q9BZS1); MKI67 (P46013); ULBP2 (Q9BZM5). These proteins were detected by flow cytometry using the antibodies listed in Table S2. The accession numbers from GenBank (http://www.ncbi.nlm.nih.gov/genbank) for the viruses mentioned in the text are as follows: HIV-1 strain JR-CSF (M38429.1); HIV-1 strain NL4-3 (M19921.2).

Supporting Information

Figure S1 Depletion of Treg by WT HIV-1 infection. The percentage of $FOXP3^+$ $CD4^-$ cells in splenic MNCs of WT HIV-1-infected mice (n = 5) and mock-infected mice (n = 5) at 21 dpi are shown. Representative dot plots are shown below. The numbers under the dot plots correspond to the percentage in each quadrant. NS, no statistical significance.
(TIF)

Figure S2 Infectivity of R5 WT and *vpr*-deficient HIV-1. R5 WT and *vpr*-deficient HIV-1 (strain JR-CSF) were prepared as described in Materials and Methods. (Top) Western blot analyses of the virions. (Bottom) TZM-bl assay. Prepared virus solutions were inoculated into TZM-bl indicator cells. The infectivities of these viruses were quantified as described in Materials and Methods and were normalized to the amount of p24. The assay was performed in triplicate. NS, no statistical significance.
(TIF)

Figure S3 Infectivity of X4 WT and *vpr*-deficient HIV-1. X4 WT and *vpr*-deficient HIV-1 (strain NL4-3) were prepared as described in Materials and Methods. (Top) Western blot analyses of the virions. (Bottom) TZM-bl assay. Prepared virus solutions were inoculated into TZM-bl indicator cells. The infectivities of these viruses were quantified as described in Materials and Methods and were normalized to the amount of p24. The assay was performed in triplicate. NS, no statistical significance.
(TIF)

Figure S4 No association of ULBP2 with the Treg depletion observed in WT HIV-1-infected mice. Splenic MNCs of WT HIV-1-infected mice (n = 7), *vpr*-deficient HIV-1-infected mice (n = 7), and mock-infected mice (n = 7) at 7 dpi were analyzed by flow cytometry using an anti-ULBP2 and an anti-HIV-1 p24 antibodies. The percentages of $ULBP2^+$ cells in $CD3^+$ $CD8^-$ cells (A) and in each population (B) are respectively shown. Representative histograms are shown on the right. The numbers in histogram indicate the percentage of active $CASP3^+$ cells in each population. Statistical difference was determined by Welch's t test. NS, no statistical significance.
(TIF)

Figure S5 Expansion of memory $CD8^+$ T cells in DD-treated humanized mice. The numbers of total $CD8^+$ T cells ($CD45^+$ $CD3^+$ $CD8^+$ cells), naïve $CD8^+$ T cells ($CD45^+$ $CD3^+$ $CD8^+$ $CD45RA^+$ cells), and memory $CD8^+$ T cells ($CD45^+$ $CD3^+$ $CD8^+$ $CD45RA^-$ cells) in the PB of R5 WT HIV-1-infected DD-treated mice (n = 13), R5 *vpr*-deficient HIV-1-infected DD-treated mice (n = 13), and mock-infected DD-treated mice (n = 8) were routinely quantified by flow cytometry and hematocytometry.
(TIF)

Table S1 Humanized mice used in this study. A full list of the 132 humanized mice used in this study.
(PDF)

Table S2 Antibodies used in flow cytometry analyses. A full list of antibodies used in this study.
(PDF)

Acknowledgments

We would like to thank Peter Gee (Institute for Virus Research, Kyoto University, Japan) and Keiko Okano (Research Administration Office, Kyoto University, Japan) for proofreading this manuscript, Yoshinori Fukazawa (Oregon Health and Science University, United States of America), Rob J. de Boer (Utrecht University, the Netherland), Shimon Sakaguchi, and Motonao Osaki (Institute for Medical Sciences, Kyoto University, Japan) for helpful suggestions and discussion, and Yuetsu Tanaka (University of the Ryukyus, Japan) and Akio Adachi (The University of Tokushima) for providing materials. We also thank all the members in the laboratory of Virus Pathogenesis, Institute for Virus Research, Kyoto University for lively discussion and Kotubu Misawa for the dedicated support.

Author Contributions

Conceived and designed the experiments: KS YK. Performed the experiments: KS NM YS. Analyzed the data: KS NM SI YS MM. Contributed reagents/materials/analysis tools: SI MM YI MI KA DSA. Wrote the paper: KS YK.

References

1. Andersen JL, Le Rouzic E, Planelles V (2008) HIV-1 Vpr: mechanisms of G2 arrest and apoptosis. Exp Mol Pathol 85: 2–10.
2. Ogawa K, Shibata R, Kiyomasu T, Higuchi I, Kishida Y, et al. (1989) Mutational analysis of the human immunodeficiency virus *vpr* open reading frame. J Virol 63: 4110–4114.
3. Gummuluru S, Emerman M (1999) Cell cycle- and Vpr-mediated regulation of human immunodeficiency virus type 1 expression in primary and transformed T-cell lines. J Virol 73: 5422–5430.
4. Eckstein DA, Sherman MP, Penn ML, Chin PS, De Noronha CM, et al. (2001) HIV-1 Vpr enhances viral burden by facilitating infection of tissue macrophages but not nondividing $CD4^+$ T cells. J Exp Med 194: 1407–1419.
5. Hoch J, Lang SM, Weeger M, Stahl-Hennig C, Coulibaly C, et al. (1995) *vpr* deletion mutant of simian immunodeficiency virus induces AIDS in rhesus monkeys. J Virol 69: 4807–4813.
6. Stevenson M (2003) HIV-1 pathogenesis. Nat Med 9: 853–860.
7. Sakaguchi S, Miyara M, Costantino CM, Hafler DA (2010) $FOXP3^+$ regulatory T cells in the human immune system. Nat Rev Immunol 10: 490–500.
8. Hori S, Nomura T, Sakaguchi S (2003) Control of regulatory T cell development by the transcription factor Foxp3. Science 299: 1057–1061.
9. Fisson S, Darrasse-Jeze G, Litvinova E, Septier F, Klatzmann D, et al. (2003) Continuous activation of autoreactive $CD4^+CD25^+$ regulatory T cells in the steady state. J Exp Med 198: 737–746.
10. Vukmanovic-Stejic M, Zhang Y, Cook JE, Fletcher JM, McQuaid A, et al. (2006) Human $CD4^+CD25^{hi}Foxp3^+$ regulatory T cells are derived by rapid turnover of memory populations in vivo. J Clin Invest 116: 2423–2433.
11. Miyara M, Yoshioka Y, Kitoh A, Shima T, Wing K, et al. (2009) Functional delineation and differentiation dynamics of human $CD4^+$ T cells expressing the FoxP3 transcription factor. Immunity 30: 899–911.
12. Dittmer U, He H, Messer RJ, Schimmer S, Olbrich AR, et al. (2004) Functional impairment of $CD8^+$ T cells by regulatory T cells during persistent retroviral infection. Immunity 20: 293–303.
13. Weiss L, Donkova-Petrini V, Caccavelli L, Balbo M, Carbonneil C, et al. (2004) Human immunodeficiency virus-driven expansion of $CD4^+CD25^+$ regulatory T cells, which suppress HIV-specific CD4 T-cell responses in HIV-infected patients. Blood 104: 3249–3256.
14. Holmes D, Jiang Q, Zhang L, Su L (2008) Foxp3 and Treg cells in HIV-1 infection and immuno-pathogenesis. Immunol Res 41: 248–266.
15. Oswald-Richter K, Grill SM, Shariat N, Leelawong M, Sundrud MS, et al. (2004) HIV infection of naturally occurring and genetically reprogrammed human regulatory T-cells. PLoS Biol 2: E198.
16. Apoil PA, Puissant B, Roubinet F, Abbal M, Massip P, et al. (2005) FOXP3 mRNA levels are decreased in peripheral blood $CD4^+$ lymphocytes from HIV-positive patients. J Acquir Immune Defic Syndr 39: 381–385.
17. Eggena MP, Barugahare B, Jones N, Okello M, Mutalya S, et al. (2005) Depletion of regulatory T cells in HIV infection is associated with immune activation. J Immunol 174: 4407–4414.
18. Pereira LE, Villinger F, Onlamoon N, Bryan P, Cardona A, et al. (2007) Simian immunodeficiency virus (SIV) infection influences the level and function of regulatory T cells in SIV-infected rhesus macaques but not SIV-infected sooty mangabeys. J Virol 81: 4445–4456.
19. Chase AJ, Yang HC, Zhang H, Blankson JN, Siliciano RF (2008) Preservation of $FoxP3^+$ regulatory T cells in the peripheral blood of human immunodeficiency virus type 1-infected elite suppressors correlates with low $CD4^+$ T-cell activation. J Virol 82: 8307–8315.
20. Favre D, Lederer S, Kanwar B, Ma ZM, Proll S, et al. (2009) Critical loss of the balance between Th17 and T regulatory cell populations in pathogenic SIV infection. PLoS Pathog 5: e1000295.
21. Nie C, Sato K, Misawa N, Kitayama H, Fujino H, et al. (2009) Selective infection of $CD4^+$ effector memory T lymphocytes leads to preferential depletion of memory T lymphocytes in R5 HIV-1-infected humanized NOD/SCID/IL-$2R\gamma^{null}$ mice. Virology 394: 64–72.
22. Sato K, Izumi T, Misawa N, Kobayashi T, Yamashita Y, et al. (2010) Remarkable lethal G-to-A mutations in *vif*-proficient HIV-1 provirus by individual APOBEC3 proteins in humanized mice. J Virol 84: 9546–9556.
23. Sato K, Misawa N, Fukuhara M, Iwami S, An DS, et al. (2012) Vpu augments the initial burst phase of HIV-1 propagation and downregulates BST2 and CD4 in humanized mice. J Virol 86: 5000–5013.
24. Sato K, Misawa N, Nie C, Satou Y, Iwakiri D, et al. (2011) A novel animal model of Epstein-Barr virus-associated hemophagocytic lymphohistiocytosis in humanized mice. Blood 117: 5663–5673.
25. Sato K, Nie C, Misawa N, Tanaka Y, Ito M, et al. (2010) Dynamics of memory and naive $CD8^+$ T lymphocytes in humanized NOD/SCID/IL-$2R\gamma^{null}$ mice infected with CCR5-tropic HIV-1. Vaccine 28 Suppl 2: B32–37.
26. Billerbeck E, Barry WT, Mu K, Dorner M, Rice CM, et al. (2011) Development of human $CD4^+FoxP3^+$ regulatory T cells in human stem cell factor-, granulocyte-macrophage colony-stimulating factor-, and interleukin-3-expressing NOD-SCID IL2Rγ^{null} humanized mice. Blood 117: 3076–3086.
27. Duan K, Zhang B, Zhang W, Zhao Y, Qu Y, et al. (2011) Efficient peripheral construction of functional human regulatory $CD4^+CD25^{high}Foxp3^+$ T cells in NOD/SCID mice grafted with fetal human thymus/liver tissues and $CD34^+$ cells. Transpl Immunol 25: 173–179.
28. Jiang Q, Zhang L, Wang R, Jeffrey J, Washburn ML, et al. (2008) $FoxP3^+CD4^+$ regulatory T cells play an important role in acute HIV-1 infection in humanized *Rag2*$^{-/-}\gamma C^{-/-}$ mice in vivo. Blood 112: 2858–2868.
29. Onoe T, Kalscheuer H, Danzl N, Chittenden M, Zhao G, et al. (2011) Human natural regulatory T cell development, suppressive function, and postthymic maturation in a humanized mouse model. J Immunol 187: 3895–3903.
30. Koyanagi Y, Miles S, Mitsuyasu RT, Merrill JE, Vinters HV, et al. (1987) Dual infection of the central nervous system by AIDS viruses with distinct cellular tropisms. Science 236: 819–822.
31. Bofill M, Mocroft A, Lipman M, Medina E, Borthwick NJ, et al. (1996) Increased numbers of primed activated $CD8^+CD38^+CD45RO^+$ T cells predict the decline of $CD4^+$ T cells in HIV-1-infected patients. AIDS 10: 827–834.
32. Benito JM, Lopez M, Lozano S, Martinez P, Gonzalez-Lahoz J, et al. (2004) CD38 expression on CD8 T lymphocytes as a marker of residual virus replication in chronically HIV-infected patients receiving antiretroviral therapy. AIDS Res Hum Retroviruses 20: 227–233.
33. Kawano Y, Tanaka Y, Misawa N, Tanaka R, Kira JI, et al. (1997) Mutational analysis of human immunodeficiency virus type 1 (HIV-1) accessory genes: requirement of a site in the nef gene for HIV-1 replication in activated $CD4^+$ T cells *in vitro* and *in vivo*. J Virol 71: 8456–8466.
34. Adachi A, Gendelman HE, Koenig S, Folks T, Willey R, et al. (1986) Production of acquired immunodeficiency syndrome-associated retrovirus in human and nonhuman cells transfected with an infectious molecular clone. J Virol 59: 284–291.
35. Goh WC, Rogel ME, Kinsey CM, Michael SF, Fultz PN, et al. (1998) HIV-1 Vpr increases viral expression by manipulation of the cell cycle: a mechanism for selection of Vpr *in vivo*. Nat Med 4: 65–71.
36. Vieillard V, Strominger JL, Debre P (2005) NK cytotoxicity against $CD4^+$ T cells during HIV-1 infection: a gp41 peptide induces the expression of an NKp44 ligand. Proc Natl Acad Sci U S A 102: 10981–10986.
37. Chang JJ, Altfeld M (2010) Innate immune activation in primary HIV-1 infection. J Infect Dis 202 Suppl 2: S297–301.
38. Ward J, Davis Z, DeHart J, Zimmerman E, Bosque A, et al. (2009) HIV-1 Vpr triggers natural killer cell-mediated lysis of infected cells through activation of the ATR-mediated DNA damage response. PLoS Pathog 5: e1000613.
39. Richard J, Sindhu S, Pham TN, Belzile JP, Cohen EA (2010) HIV-1 Vpr up-regulates expression of ligands for the activating NKG2D receptor and promotes NK cell-mediated killing. Blood 115: 1354–1363.
40. Stevenson M, Stanwick TL, Dempsey MP, Lamonica CA (1990) HIV-1 replication is controlled at the level of T cell activation and proviral integration. EMBO J 9: 1551–1560.
41. Zack JA, Arrigo SJ, Weitsman SR, Go AS, Haislip A, et al. (1990) HIV-1 entry into quiescent primary lymphocytes: molecular analysis reveals a labile, latent viral structure. Cell 61: 213–222.
42. Salazar-Gonzalez JF, Salazar MG, Keele BF, Learn GH, Giorgi EE, et al. (2009) Genetic identity, biological phenotype, and evolutionary pathways of transmitted/founder viruses in acute and early HIV-1 infection. J Exp Med 206: 1273–1289.
43. Jowett JB, Planelles V, Poon B, Shah NP, Chen ML, et al. (1995) The human immunodeficiency virus type 1 vpr gene arrests infected T cells in the G2+M phase of the cell cycle. J Virol 69: 6304–6313.
44. Rogel ME, Wu LI, Emerman M (1995) The human immunodeficiency virus type 1 *vpr* gene prevents cell proliferation during chronic infection. J Virol 69: 882–888.
45. Parrish NF, Wilen CB, Banks LB, Iyer SS, Pfaff JM, et al. (2012) Transmitted/founder and chronic subtype C HIV-1 use CD4 and CCR5 receptors with equal efficiency and are not inhibited by blocking the integrin $\alpha4\beta7$. PLoS Pathog 8: e1002686.
46. Keele BF, Giorgi EE, Salazar-Gonzalez JF, Decker JM, Pham KT, et al. (2008) Identification and characterization of transmitted and early founder virus envelopes in primary HIV-1 infection. Proc Natl Acad Sci U S A 105: 7552–7557.
47. Koot M, van 't Wout AB, Kootstra NA, de Goede RE, Tersmette M, et al. (1996) Relation between changes in cellular load, evolution of viral phenotype, and the clonal composition of virus populations in the course of human immunodeficiency virus type 1 infection. J Infect Dis 173: 349–354.
48. Mosier DE (2009) How HIV changes its tropism: evolution and adaptation? Curr Opin HIV AIDS 4: 125–130.
49. Brenchley JM, Silvestri G, Douek DC (2010) Nonprogressive and progressive primate immunodeficiency lentivirus infections. Immunity 32: 737–742.
50. Brenchley JM, Schacker TW, Ruff LE, Price DA, Taylor JH, et al. (2004) $CD4^+$ T cell depletion during all stages of HIV disease occurs predominantly in the gastrointestinal tract. J Exp Med 200: 749–759.
51. Veazey RS, DeMaria M, Chalifoux LV, Shvetz DE, Pauley DR, et al. (1998) Gastrointestinal tract as a major site of $CD4^+$ T cell depletion and viral replication in SIV infection. Science 280: 427–431.
52. Giavedoni LD, Velasquillo MC, Parodi LM, Hubbard GB, Hodara VL (2000) Cytokine expression, natural killer cell activation, and phenotypic changes in lymphoid cells from rhesus macaques during acute infection with pathogenic simian immunodeficiency virus. J Virol 74: 1648–1657.

53. Emilie D, Peuchmaur M, Maillot MC, Crevon MC, Brousse N, et al. (1990) Production of interleukins in human immunodeficiency virus-1-replicating lymph nodes. J Clin Invest 86: 148–159.
54. Brenchley JM, Price DA, Schacker TW, Asher TE, Silvestri G, et al. (2006) Microbial translocation is a cause of systemic immune activation in chronic HIV infection. Nat Med 12: 1365–1371.
55. Akira S, Takeda K, Kaisho T (2001) Toll-like receptors: critical proteins linking innate and acquired immunity. Nat Immunol 2: 675–680.
56. Sauter B, Albert ML, Francisco L, Larsson M, Somersan S, et al. (2000) Consequences of cell death: exposure to necrotic tumor cells, but not primary tissue cells or apoptotic cells, induces the maturation of immunostimulatory dendritic cells. J Exp Med 191: 423–434.
57. Basu S, Binder RJ, Suto R, Anderson KM, Srivastava PK (2000) Necrotic but not apoptotic cell death releases heat shock proteins, which deliver a partial maturation signal to dendritic cells and activate the NF-κB pathway. Int Immunol 12: 1539–1546.
58. Ostrand-Rosenberg S, Sinha P, Beury DW, Clements VK (2012) Cross-talk between myeloid-derived suppressor cells (MDSC), macrophages, and dendritic cells enhances tumor-induced immune suppression. Semin Cancer Biol 22: 275–281.
59. Gabrilovich DI, Nagaraj S (2009) Myeloid-derived suppressor cells as regulators of the immune system. Nat Rev Immunol 9: 162–174.
60. Gorantla S, Makarov E, Finke-Dwyer J, Gebhart CL, Domm W, et al. (2010) $CD8^+$ cell depletion accelerates HIV-1 immunopathology in humanized mice. J Immunol 184: 7082–7091.
61. Baenziger S, Tussiwand R, Schlaepfer E, Mazzucchelli L, Heikenwalder M, et al. (2006) Disseminated and sustained HIV infection in $CD34^+$ cord blood cell-transplanted $Rag2^{-/-}\gamma_c^{-/-}$ mice. Proc Natl Acad Sci U S A 103: 15951–15956.
62. Watanabe S, Ohta S, Yajima M, Terashima K, Ito M, et al. (2007) Humanized NOD/SCID/IL2Rγ^{null} mice transplanted with hematopoietic stem cells under nonmyeloablative conditions show prolonged life spans and allow detailed analysis of human immunodeficiency virus type 1 pathogenesis. J Virol 81: 13259–13264.
63. Watanabe S, Terashima K, Ohta S, Horibata S, Yajima M, et al. (2007) Hematopoietic stem cell-engrafted NOD/SCID/IL2Rγ^{null} mice develop human lymphoid systems and induce long-lasting HIV-1 infection with specific humoral immune responses. Blood 109: 212–218.
64. Sato K, Koyanagi Y (2011) The mouse is out of the bag: insights and perspectives on HIV-1-infected humanized mouse models. Exp Biol Med (Maywood) 236: 977–985.
65. Berges BK, Rowan MR (2011) The utility of the new generation of humanized mice to study HIV-1 infection: transmission, prevention, pathogenesis, and treatment. Retrovirology 8: 65.
66. Shultz LD, Brehm MA, Garcia-Martinez JV, Greiner DL (2012) Humanized mice for immune system investigation: progress, promise and challenges. Nat Rev Immunol 12: 786–798.
67. Levy DN, Refaeli Y, MacGregor RR, Weiner DB (1994) Serum Vpr regulates productive infection and latency of human immunodeficiency virus type 1. Proc Natl Acad Sci U S A 91: 10873–10877.
68. Hoshino S, Sun B, Konishi M, Shimura M, Segawa T, et al. (2007) Vpr in plasma of HIV type 1-positive patients is correlated with the HIV type 1 RNA titers. AIDS Res Hum Retroviruses 23: 391–397.
69. Zimmerman ES, Sherman MP, Blackett JL, Neidleman JA, Kreis C, et al. (2006) Human immunodeficiency virus type 1 Vpr induces DNA replication stress *in vitro* and *in vivo*. J Virol 80: 10407–10418.
70. Sakai K, Dimas J, Lenardo MJ (2006) The Vif and Vpr accessory proteins independently cause HIV-1-induced T cell cytopathicity and cell cycle arrest. Proc Natl Acad Sci U S A 103: 3369–3374.
71. Wang J, Shackelford JM, Casella CR, Shivers DK, Rapaport EL, et al. (2007) The Vif accessory protein alters the cell cycle of human immunodeficiency virus type 1 infected cells. Virology 359: 243–252.
72. Izumi T, Io K, Matsui M, Shirakawa K, Shinohara M, et al. (2010) HIV-1 viral infectivity factor interacts with TP53 to induce G2 cell cycle arrest and positively regulate viral replication. Proc Natl Acad Sci U S A 107: 20798–20803.
73. Ito M, Hiramatsu H, Kobayashi K, Suzue K, Kawahata M, et al. (2002) NOD/SCID/γ_c^{null} mouse: an excellent recipient mouse model for engraftment of human cells. Blood 100: 3175–3182.
74. An DS, Poon B, Ho Tsong Fang R, Weijer K, Blom B, et al. (2007) Use of a novel chimeric mouse model with a functionally active human immune system to study human immunodeficiency virus type 1 infection. Clin Vaccine Immunol 14: 391–396.

Cell Host & Microbe
Article

Antimicrobial Peptide LL-37 Produced by HSV-2-Infected Keratinocytes Enhances HIV Infection of Langerhans Cells

Youichi Ogawa,[1] Tatsuyoshi Kawamura,[1,*] Takamitsu Matsuzawa,[1] Rui Aoki,[1] Peter Gee,[4] Atsuya Yamashita,[2] Kohji Moriishi,[2] Kenshi Yamasaki,[3] Yoshio Koyanagi,[4] Andrew Blauvelt,[5] and Shinji Shimada[1]
[1]Department of Dermatology
[2]Department of Microbiology
Faculty of Medicine, University of Yamanashi, Yamanashi 409-3898, Japan
[3]Department of Dermatology, Tohoku University Graduate School of Medicine, Sendai 980-8575, Japan
[4]Laboratory of Viral Pathogenesis, Institute for Virus Research, Kyoto University, Kyoto 606-8507, Japan
[5]Oregon Medical Research Center, Portland, OR 97223, USA
*Correspondence: tkawa@yamanashi.ac.jp
http://dx.doi.org/10.1016/j.chom.2012.12.002

SUMMARY

Herpes simplex virus (HSV)-2 shedding is associated with increased risk for sexually acquiring HIV. Because Langerhans cells (LCs), the mucosal epithelium resident dendritic cells, are suspected to be one of the initial target cell types infected by HIV following sexual exposure, we examined whether and how HSV-2 affects HIV infection of LCs. Although relatively few HSV-2/HIV-coinfected LCs were detected, HSV-2 dramatically enhanced the HIV susceptibility of LCs within skin explants. HSV-2 stimulated epithelial cell production of antimicrobial peptides (AMPs), including human β defensins and LL-37. LL-37 strongly upregulated the expression of HIV receptors in monocyte-derived LCs (mLCs), thereby enhancing their HIV susceptibility. Culture supernatants of epithelial cells infected with HSV-2 enhanced HIV susceptibility in mLCs, and this effect was abrogated by blocking LL-37 production. These data suggest that HSV-2 enhances sexual transmission of HIV by increasing HIV susceptibility of LCs via epithelial cell production of LL-37.

INTRODUCTION

Epidemiologic studies have indicated a strong association between the acquisition of HIV and other sexually transmitted diseases (STDs) (Galvin and Cohen, 2004). This link is especially evident in cases of genital ulcer diseases (GUDs), with a 2- to 11-fold increase in the rate of HIV acquisition in the presence of GUD (Cameron et al., 1989; Fleming and Wasserheit, 1999). It is widely recognized that herpes simplex virus type 2 (HSV-2) is a major cause of GUDs, and more than 50 epidemiologic studies have now indicated that HSV-2 shedding is associated with increased risk for acquiring HIV (Wald and Link, 2002). The risk ratio of HIV acquisition for a person with genital herpes is enhanced from 2 to 4 when compared with a person without genital herpes, and potentially 50% of new HIV infections are considered to be attributable or worsened by HSV-2 infection (Wald and Link, 2002).

During sexual transmission of HIV, virus crosses mucosal epithelium and is eventually transmitted to regional lymph nodes, where it establishes permanent infection. Many studies have shown that Langerhans cells (LCs) are one of the important initial cellular targets for HIV, and that this particular type of dendritic cell (DC) plays a crucial role in disseminating HIV (de Witte et al., 2007; Kawamura et al., 2005; Lederman et al., 2006; Shattock and Moore, 2003). LCs are present within genital skin (e.g., outer foreskin) and mucosal epithelium and, after contact with pathogens, readily emigrate from tissue to draining lymph nodes. Immature resident LCs express surface CD4 and CCR5, but not surface CXCR4 (Zaitseva et al., 1997). These LCs are readily infected ex vivo with R5 HIV, but not with X4 HIV (Kawamura et al., 2000, 2008; Reece et al., 1998; Zaitseva et al., 1997). These findings are consistent with previous epidemiologic observations, which have found that the majority of HIV strains isolated from newly infected patients are R5 HIV strains (Zhu et al., 1993). It has been reported that persons with *CCR5* homozygous defects are largely protected from sexually acquiring HIV (Liu et al., 1996).

Clinical trials performed over the last several years have shown that circumcision greatly reduces the probability of penile HIV transmission, suggesting that the foreskin is an important portal of HIV entry (Auvert et al., 2005; Bailey et al., 2007; Gray et al., 2007). Although the mechanism leading to protection remains undefined, several ex vivo experiments with foreskin explants have indicated that CD4 T lymphocytes and LCs within foreskin epidermis are initial target cells for HIV (Fahrbach et al., 2010; Ganor et al., 2010; Grivel et al., 2011; Zhou et al., 2011).

In primate models of simian immunodeficiency virus (SIV) infection, there is controversy regarding which cells in the genital mucosa are initially infected by SIV. Studies have demonstrated that the primary infected cells present in the lamina propria of the cervicovaginal mucosa 48–72 hr after intravaginal exposure to SIV are T cells or submucosal DCs, but not epithelial LCs (Spira et al., 1996; Zhang et al., 1999). When vaginal tissue was examined within 1 hr following vaginal inoculation, however, up to

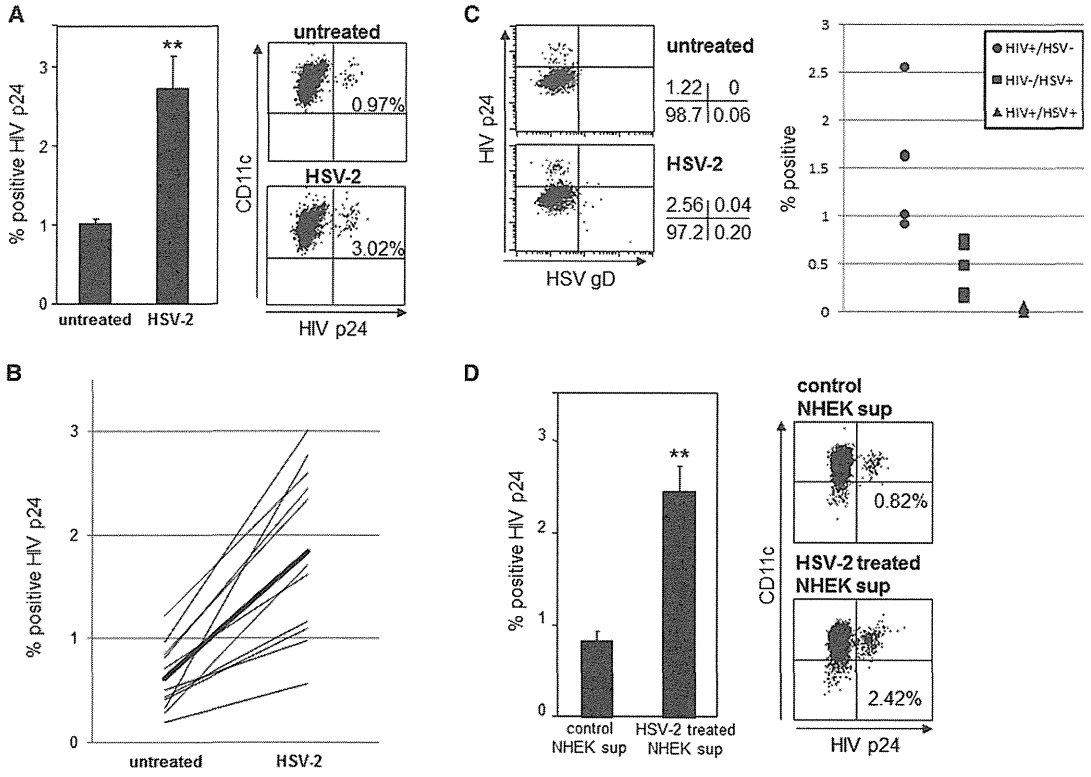

Figure 1. HSV-2-Infected Epithelial Cells Augment HIV Infection in LCs

(A–C) Epithelial sheets were preincubated with HSV-2 and then exposed to R5 HIV. Epithelial sheets were floated on culture medium to allow migration of LCs from the explants. Emigrating cells from the epidermal sheets were collected 3 days following HIV exposure. HIV-infected LCs were assessed by HIV p24 intracellular staining in langerin$^+$ CD11c$^+$ LCs (A) and the results of 11 separate experiments with different donors are summarized (B). HSV− and/or HIV-infected LCs were assessed by HIV p24 and HSV gD intracellular staining in CD11c$^+$ LCs, and the results from five different donors are summarized (C).

(D) mLCs were preincubated with the supernatants from NHEKs treated with or without HSV-2, and then exposed to R5 HIV. HIV p24$^+$ cells were assessed in langerin$^+$ CD11c$^+$ mLCs at day 7.

(A, C, and D) Representative flow cytometric analyses are shown. (A and D) Results are shown as means ± SD (n = 3) (**$p < 0.01$). See also Figure S1.

90% of SIV-infected cells were found to be LCs (Hu et al., 2000). Because only a single layer of columnar epithelium guards the endocervix and the transformation zone, the mucosal barrier can be easily breached by mechanisms such as the microtrauma associated with sexual intercourse, which provides immediate access to target cells, especially CD4$^+$ T cells, in the submucosa (Haase, 2010). Indeed, it has been shown that following mucosal exposure to high doses of SIV, virus can gain access through breaks in the mucosal epithelial barrier and infect resting CD4$^+$ T cells in the submucosa (Haase, 2010). Since molecules targeting CCR5 completely protected against mucosal transmission of SHIV (Lederman et al., 2004), CD4/CCR5-mediated de novo infection of LCs and/or CD4$^+$ T cells is considered to be a major pathway involved in sexual transmission of HIV.

Several mechanisms have been proposed to explain enhanced sexual transmission of HIV during active STD infection, including breakdown of epithelial barriers (i.e., ulceration) with direct inoculation of HIV into the blood (Cunningham et al., 1985), presence of inflammatory leukocytes that act as targets (Zhu et al., 2009), and coinfection of cells by HIV and STD pathogens. Biological mechanisms responsible for greater HIV transmission rates in the presence of genital herpes infections, however, are as of yet unknown. Recently, we and others have suggested that HIV susceptibility of LCs could be directly enhanced by pathogens and indirectly enhanced by inflammatory factors during STD, thereby leading to more likely sexual transmission of HIV (de Jong et al., 2008; Ogawa et al., 2009). In this report, we found that HSV-2 primarily infected epithelial cells and then markedly enhanced HIV infection in adjacent LCs. Interestingly, mechanistic studies revealed that LL-37 produced by HSV-2-infected epithelial cells upregulated CD4 and CCR5 on the surface of bystander LCs, thereby enhancing HIV infection in these cells. These findings may lead to new strategies designed to block sexual transmission of HIV.

RESULTS

HSV-2 Indirectly Enhances HIV Susceptibility in LCs via Interaction with Epithelial Cells

We first examined whether HSV-2 modulates HIV susceptibility of LCs by using an ex vivo skin explant model, whereby resident LCs within epithelial tissue are exposed to HIV and then allowed to emigrate from tissue, thus mimicking conditions that occur following mucosal exposure to HIV (Kawamura et al., 2000).